Study of Structural, Dielectric and Gas Sensing Properties of Nickel Doped Magnesium Ferrites

Samira Yasmin

NUST201361979MSNS78113F

This thesis is submitted as a partial fulfillment of the requirements for the degree of

M.Phil Physics

Supervisor: Dr. Iftikhar Hussain Gul

**School of Natural Sciences (SNS)
National University of Sciences and
Technology (NUST), H-12
Islamabad, Pakistan**

September, 2017

National University of Sciences & Technology

M.Phil THESIS WORK

We hereby recommend that the dissertation prepared under our supervision by: Samira Yasmin, Regn No. NUST201361979MSNS78113F Titled: **Study of Structural, Dielectric and Gas Sensing Properties of Nickel Doped Magnesium Ferrites** be accepted in partial fulfillment of the requirements for the award of **M.Phil** degree.

Examination Committee Members

1. Name: Dr. Zakir Hussain   Signature: _____

2. Name: Dr. Faheem Amin   Signature: _____

3. Name: _____   Signature: _____

4. Name: Dr. Muhammad Mumtaz   Signature: _____

Supervisor's Name: Dr. Iftikhar H. Gul   Signature: _____

_____
Head of Department

05/09/17
Date

COUNTERSINGED

Date: 05/09/2017

_____
Dean/Principal

THESIS ACCEPTANCE CERTIFICATE

Certified that final copy of MS/M.Phil thesis written by **Ms. Samira Yasmin**, (Registration No. **NUST201361979MSNS78113F**), of **School of Natural Sciences** has been vetted by undersigned, found complete in all respects as per NUST statutes/regulations, is free of plagiarism, errors, and mistakes and is accepted as partial fulfillment for award of MS/M.Phil degree. It is further certified that necessary amendments as pointed out by GEC members and external examiner of the scholar have also been incorporated in the said thesis.

Signature: _____

Name of Supervisor: Dr. Iftikhar Hussain Gul

Date: _____05-09-2017_____

Signature (HoD): _____

Date: _____05/09/17_____

Signature (Dean/Principal): _____

Date: _____05/09/2017_____

To my wonderful parents

Acknowledgements

Abstract

Nickel was substituted in magnesium ferrites in four different percentages using the simple synthesis approach of co-precipitation. Nickel nitrate, iron nitrate, magnesium nitrate and sodium hydroxide were utilized for the preparation of $Mg_{1-x}Ni_xFe_2O_4$ (x=0, 0.2, 0.35 and 0.5). Face centered cubic structure of the spinel ferrites was confirmed through the X-ray Diffraction (XRD) technique with no extra peaks. Crystallite sizes of the prepared samples were in the range of 4.17-8.36 nm. Lattice parameter was calculated and it showed a decreasing trend with increase in the doping concentration. Mass densities and x-ray densities increased with increase in Ni^{2+} content. The morphology of nanoferrites was examined through Scanning Electron Microscopy (SEM). SEM images showed homogeneous arrangement of particles along with little agglomeration somewhere. Particles of small size were observed in the SEM images. Average particle size of the samples $MgFe_2O_4$, $Mg_{0.8}Ni_{0.2}Fe_2O_4$, $Mg_{0.65}Ni_{0.35}Fe_2O_4$ and $Mg_{0.5}Ni_{0.5}Fe_2O_4$ are 25.6 nm, 23.6 nm, 23.4 nm and 48.5 nm respectively. Powdered Potassium Bromide (KBr) and ferrite samples were compressed to pellets for analysis using Fourier Transformed Infrared (FTIR) Spectroscopy. It confirmed the formation of spinel structure by showing the metal-oxygen bonds at the octahedral and tetrahedral sites. Pellets of the powdered samples were made for studying the dielectric and gas sensing properties. Dielectric constant and dielectric loss showed a decreasing trend with increase in frequency. The prepared pellets were tested for sensing of N_2, O_2 and methane gases. The resistance of samples was measured as a function of time and sensitivity was calculated using a relation. $Mg_{1-x}Ni_xFe_2O_4$ showed greater sensitivity towards methane gas. The prepared ferrites were found to be potential candidates to be used as gas sensors for a few number of gases. Sensitivity of these ferrites with different compositions can also be examined. The response of prepared ferrites towards other gases could be analyzed also. The presence of harmful gases can be detected using the ferrite gas sensors.

Contents

List of Figures

List of Tables

List of Abbreviations

Ni	Nickel
Mg	Magnesium
Fe	Iron
O	Oxygen
XRD	X-ray Diffractometry
nm	Nano meter
SEM	Scanning Electrons Microscope
FTIR	Fourier Transform Infrared
AC	Alternating Current
χ	Magnetic Susceptibility
R	Rare Earth Trivalent Cations
Y	Yttrium
La	Lanthanum
Gd	Gadolinium
Ca	Calcium
Si	Silicon
YIG	Yttrium Iron Garnet
Ba	Barium
Sr	Strontium
Pb	Lead
Zn	Zinc
Co	Cobalt
MRI	Magnetic Resonance Imaging
δ	Degree of Inversion
Å	Angstrom
LCR	Inductance, Capacitance, Resistance
DUT	Device Under Test
hkl	Millers Indices
IR	Infrared
DLS	Dynamic light scattering
TEM	Transmission electron microscopy
AFM	Atomic Force Microscopy
STM	Scanning Tunneling Microscopy
LSCM	Laser Scanning Confocal Microscopy
BET	Brunauer-Emmett-Teller
DSC	Differential Scanning Calorimetry

Chapter 1

Introduction

1.1 Nanoscience and Nanotechnology

The perception of nanotechnology and the probability of deploying matter at the atomic level were first brought into light in a lecture, *There's Plenty of Room at the Bottom*, held by the physicist Richard Feynman in 1959. The study of fundamental principles governing materials having at least one of their dimensions in the nano regime (1–100 nanometers), is addressed in the field of Nano-science. One nanometer (nm) is one billionth part of one meter; in daily context the scale of a nanometer can be related to one hundred thousandth of the thickness of a human hair - extremely small. By comparison, the diameter of an average human hair is approximately 100,000 nm and a red blood cell is about 7,000 nm in diameter.
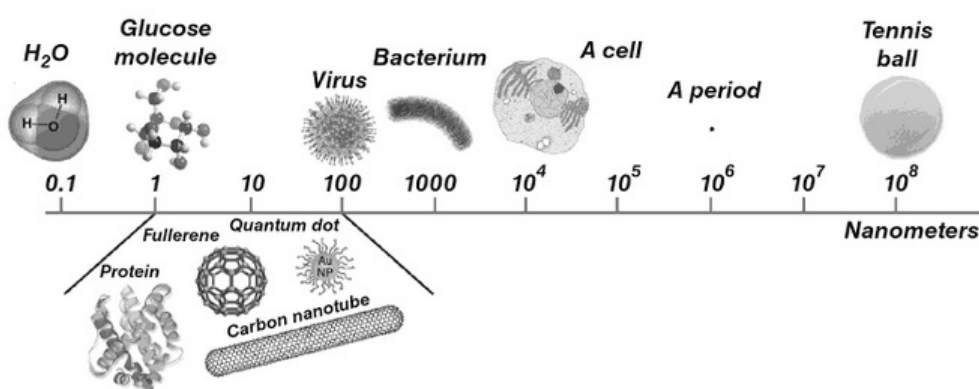
Figure 1.1: Size comparisons of objects, nanomaterials and biomolecules [1]

The properties of a material in the range of 1–100 nm, can be different from the properties of the same material at larger size. At the nano range, variation of properties occurs because, surface area increases and dominance of quantum effects occurs. Increased surface area of nano-structures results in an increase in their chemical reactivity. At

sizes of tens of nanometers, optical, magnetic or electrical properties of a material can significantly change due to quantum effects. Change in properties at the nanometer scale as compared to their bulk counter parts is observed due to increased surface area to volume ratio [2].

In Nanotechnology, nano-structures are applied into constructive nanoscale devices. Nanotechnology deals with the design, fabrication and characterization of nanostructures and systems. The possibility of controlling fundamental characteristics of a material by synthesizing nanoscale structure exists [3]. Pioneers of the extensive modern age activities in nanoscience and nanotechnology, are actually some eminent scientists of the previous century. Among those scientists, Richard P. Feynman, a novel physicist requires special mentioning. Norio Taniguchi defined nanotechnology in 1974. K. Eric Drexler promoted the concept of nanotechnology [4].

1.1.1 Nanomaterials' Classification

Nanomaterials are extremely small with at least one dimension within 100 nm scale [5]. Classification of nanomaterials in the below mentioned categories is based on dimensionality. Nanomaterials are classified on the basis of number of dimmensions in the material that are not limited to the nanoscale range (< 100 nm).

1.1.1.1 Zero-dimensional Nanomaterials

Materials categorized in this group, have all dimensions within the nanoscale. In other words no (or zero) dimension in a 0-D nanomaterial is greater than 100 nm. Figure 1.2 depicts the same.
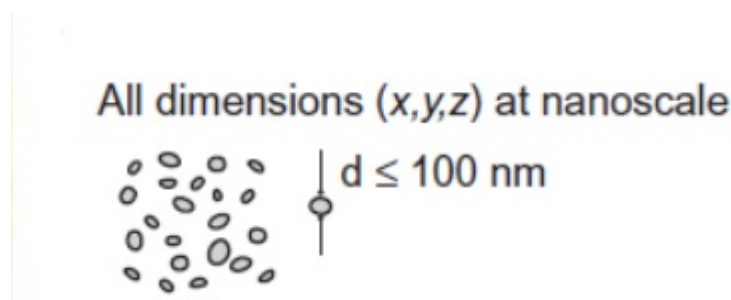
Figure 1.2: 0-D nanomaterial [6]

Nanoparticles are the most common representation of 0-D nanomaterials. General features of nanoparticles can be summarized as

- Structure of nanoparticles can be amorphous or crystalline.

- Nanoparticle having crystalline structure can be single crystalline or polycrystalline.
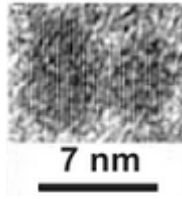
Figure 1.3: TEM image of a ZnO nanoparticle [7]

- Composition of nanoparticles can be single as well as multi-chemical elements based.

- Nanoparticles can be of various shapes and forms.

- Nanoparticles can exist individually and can also be incorporated in a matrix.

- Nanoparticles can be metallic, polymeric, and ceramic in nature.

1.1.1.2 One-dimensional Nanomaterials

Materials categorized in this group, have two dimensions within the nanoscale. In other words one dimension in a 1-D nanomaterial is greater than 100 nm. Figure 1.3 depicts the same.
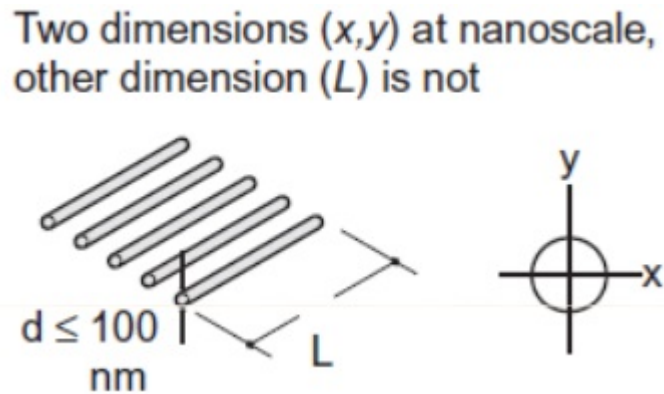
Figure 1.4: 1-D nanomaterial [6]

Examples of 1-D nanomaterials include nanowires, nanotubes, and nanorods. General features of 1-D nanomaterials can be summarized as

- 1-D nanomaterials have needle-like shape.

- Structure of 1-D nanomaterials can be amorphous or crystalline.

- Like nanoparticles having crystalline structure 1-D nanomaterials can be single crystalline or polycrystalline.

- 1-D nanomaterials can be chemically pure or impure.

- 1-D nanomaterials can exist standalone and can also be embedded in another medium.

- 1-D nanomaterials can be metallic, polymeric, and ceramic in nature.
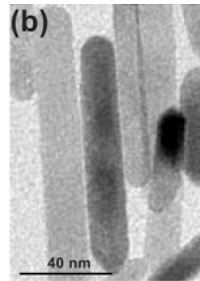
Figure 1.5: TEM image of a nanorod [7]

1.1.1.3 Two-dimensional Nanomaterials

Materials categorized in this group, have one dimension within the nanoscale. In other words two dimensions in a 2-D nanomaterial are greater than 100 nm. Figure **??** depicts the same.
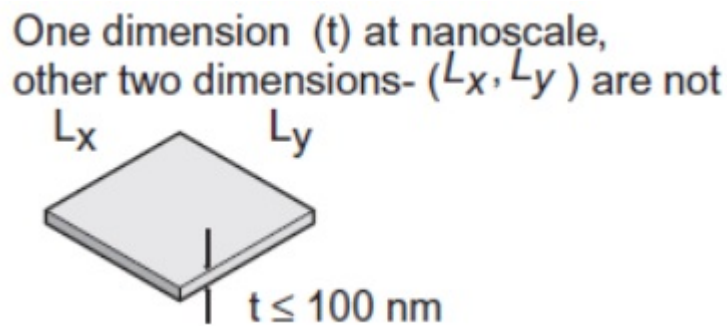
Figure 1.6: 2-D nanomaterial [6]

Examples of 2-D nanomaterials include nanolayers, nanofilms, and nancoatings. General features of 2-D nanomaterials can be summarized as

- 2-D nanomaterials have plate-like shape.

- Structure of 2-D nanomaterials can be amorphous or crystalline.

- 2-D nanomaterials can be made up by various chemical compositions.

- 2-D nanomaterials are used as single or multilayer structures.

- 2-D nanomaterials are deposited on substrates.

- 2-D nanomaterials do not exist standalone, and are integrated in a surrounding matrix material.

- 2-D nanomaterials can be metallic, polymeric, and ceramic in nature.
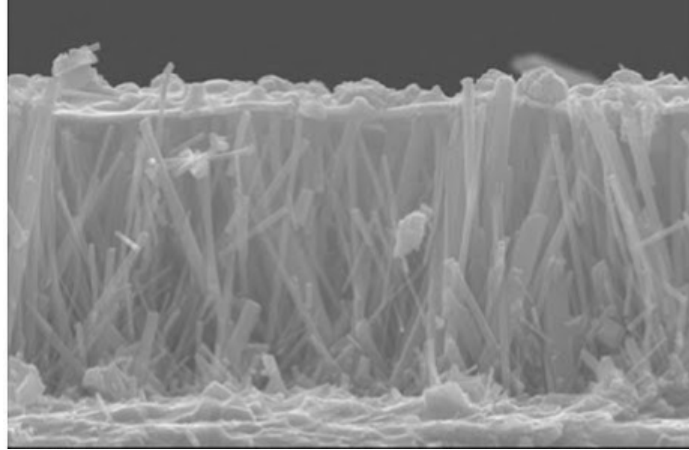
Figure 1.7: Cross sectional SEM image of a nanofilm [8]

1.1.1.4 Three-dimensional Nanomaterials

Materials categorized in this group, have no dimension within the nanoscale. In other words three dimensions in a 3-D nanomaterial are greater than 100 nm. An example is graphene nanostructure. One of the first scientific reports related to nanomaterials is the "Colloidal gold particles" synthesized by Michael Faraday in 1857 [9].

1.2 Applications of Nanotechnology

Nanotechnology is applied in many importnat applications in different fields. This widespread utility is primarily due to the distinguished properties exhibited by materials at nano scale. Figure 1.8. shows some areas of nanotechnology utility.

1.2.1 Medicine

As size of most biological structures and nanomaterials are comparable, biological applications of nanomaterial exist. The incorporation of nanomaterials with biology has developed therapy, diagnostics and drug delivery vehicles [11].

1.2.2 Energy

Nanomaterials are used in energy storage devices. The huge amount of energy required in the modern age could be attained by developing nanometer sized solar cells [12].
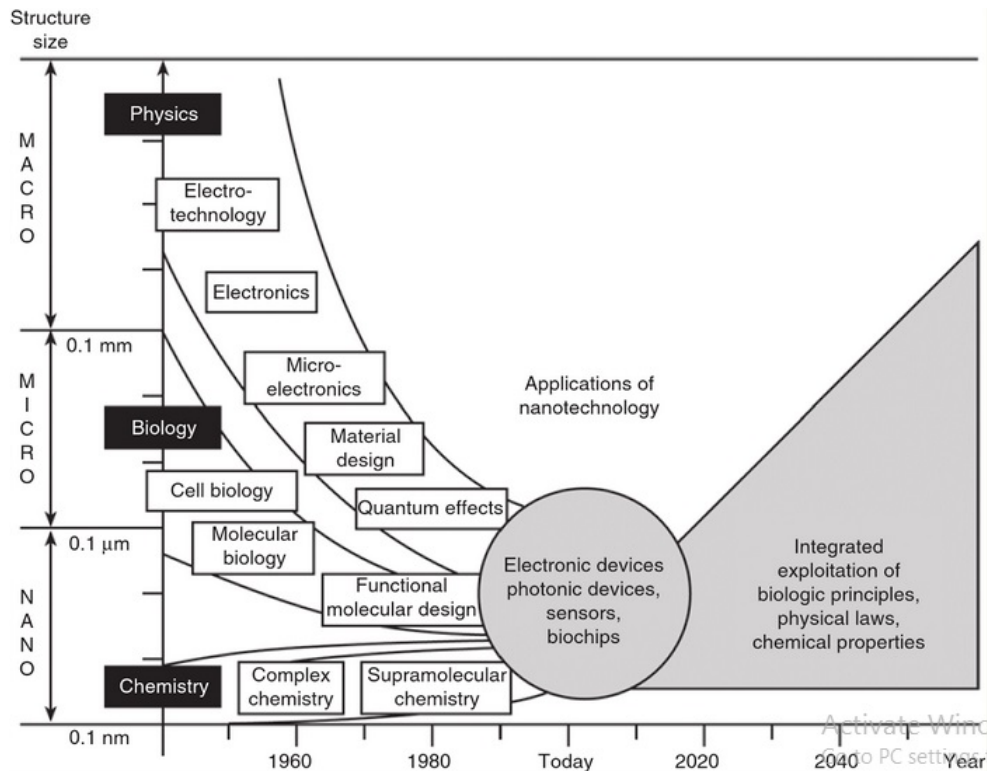
Figure 1.8: Various application fields of Nanotechnology [10]

1.2.3 Environment

Nanoporous membranes are applied to remove salts and pollutants and soften water. These membranes filter particles and micro-organisms [13]; hence having environmental applications.

1.2.4 Agriculture

Nanotechnology is believed to have the potential to provide improved techniques for treatment of crops diseases. Moreover, use of nanotechnology in fertilizers may increase crop yield [14].

1.2.5 Cosmetics

As smaller particles are easily absorbed in human skin, nanotechnology is leading to the improvement for skin care products and cosmetics beneficial for it's users [15].

1.2.6 Coatings and Paints

Nanotechnology is used to enhance the quality and life of coatings and paints. This is achieved by improving their strength, scratch resistance, and water repellent characteristics. Capacitor surfaces are coated with magnetic nanoparticles [16].

1.3   Properties of Nanomaterials

At the nanoscale, properties such as melting point, color, electrical conductivity, magnetic permeability, and chemical reactivity change as a function of the size of the particle. Thus, when a material is created with dimensions within the nanoscale, its properties change significantly from larger forms of that same material. For instance, particles of gold lose their golden color and appear red or purple at the nanoscale. Hence, nanotechnology opens a new dimension of materials, were the size can be controlled and every size behaves a little different from all other sizes.

As mentioned earlier noticeable change in materials properties are observable at nano scale. Quantum confinement and increased surface area to volume ratio are the primary factors contributing to changes in nanomaterials. Modification in electronic and optical properties of a material is caused by the quantum confinement effect. This effect induces discrete energy levels for electrons, consequently the structure of electron bands are modified as compared to that of bulk. Quantum dots and quantum wires have proven to be highly useful in lasers and light emitting diodes.

Another factor that shapes the nanoscale behavior is the predominance of quantum effects that takes place as the electrons are confined by the dimensions of the nanostructure. As the size is reduced, the quantum effects starts to dominate the properties of matter, affecting the optical, electrical and magnetic behavior of materials, i.e. for the gold nanoparticles, the motion of the electrons is confined which makes the gold particles react differently with light compared to larger sized gold particles and subsequently their color changes.

Due to minuscule size of nanomaterials, they posses an extremely large surface area to volume ratio. Consequently the number of inter-facial atoms in a nanomaterial is high. Therefore, in comparison to bulk, nanomaterials have enhanced surface properties. Chemical sensors fabricated from nanomaterials show enhanced sensitivity and selectivity. In a similar way catalytic properties of metallic nanoparticles have been proved. Better chemical stability and enhanced mechanical strength are exhibited by nanomaterials. Carbon nanotubes are well known to possess improved mechanical properties.

One of the principal factors that causes nanomaterials to differ from larger materials is the increased relative surface area. When a particle gets smaller, the surface-to-volume ratio gradually increases, leading to an increasing proportion of atoms on the surface of the particles compared to inside. As chemical reactions occur on the surfaces, nanoma-

terials can interact with the environment more efficiently than their larger counterparts, thereby making them more chemically reactive, and potentially alter their strength and electrical properties A particle with a size of 30 nm has 5% of its atoms on its surface, whereas a particle of 3 nm has as much as 50% of its atoms on the surface. Hence, a given mass of Nano particulate material will have more atoms available on the particle surface compared to the same mass of material made up of larger particles. The atoms present in nanomaterials have higher energy as compared to atoms present in bulk structure due to larger fraction of surface atoms.

1.3.1   Electrical properties

Electrical conductivity or electrical resistivity are the major electrical properties of interest in nanomaterials. Due to minuscule size of nanomaterials, the number of electron wave modes contributing in the conduction process, drastically decrease in quantity by quantized steps. This phenomenon is evident in carbon nanotubes, in which only one electron wave mode has been observed which was responsible for conduction of the material [24]. Many methods exist for studying the electrical properties. An intersting method among them, is to apply constant voltage, measure the current passing through the nanostructure. Using resistance and sample material's dimensions, resistivity can be calculated.

1.3.2   Magnetic Properties

Gold and Platinum are examples of materials that are non-magnetic in the bulk form, whereas their nanostructures are magnetic. In their nanostructures, surface atoms are different in comparison to bulk form. It is even possible to modify them by capping the surface atoms with appropriate molecules. Physical properties of the material are enhanced by virtue of this phenomenon. Strangely, gold exhibits diamagnetic properties in the bulk shows a magnetic behaviour in the nano regime [25], while platinum becomes ferromagnetic because of the structural changes on the nano scale. It has also been established that gold nano particles can be transformed to behave as ferromagnetic material by capping its nanoparticles with appropriate molecules. What happens is that the surface charge, which is localized at the surface of the particle rises the ferromagnetic behaviour. The core of 2 nm diameter gold nano particles show paramagnetic behaviour. However, the surface of 2 nm diameter gold nano particles show ferromagnetic behaviour. Furthermore, by capping the nanoparticles, permanent magnetism has been recorded at room temperatures e.g, thiol-capped gold nano particles show a permanent magnetic behaviour at room temperature.

1.3.3 Optical Properties

Nanomaterials have significant impacts in imaging, solar cells [17], optical sensors [18], phosphor, laser [19], photocatalysis [20], sensors and biomedicine [21, 22]. In nanostructures of metals and semiconductors, the effect of shape is dramatic on optical properties. Change in size has significant impact on optical properties of semiconductors, whereas impact on metals' properties is subtle. However, when anisotropy is added to the material, the optical properties show a significant change.

1.4 Synthesis of Nanomaterials

Nanotechnology has developed several methods for synthesis of nanomaterials and fabrication of nanostructures. The synthesis methods fall in the following broad categories:

- Physical Methods

- Biological Methods

- Chemical Methods

Table 1.1 enlists various methods falling under respective categories of nanomaterial synthesis.

Physical Methods	Biological Methods	Chemical Methods
Ball milling	In bacteria	Sol-gel processing
Thermal evaporation	In fungi	Solution based synthesis
Lithography	Yeast	
Vapour phase	Using plant extracts	

Table 1.1: Nanomaterial synthesis methods

Physical and chemical methods of nanomaterial synthesis are well established and practiced in various industries. Irrespective of category in which synthesis methods are placed, there are two basic approaches to synthesize nanomaterials, described ahead. Figure 1.9 pictorially depicts the two approaches.

- **Top-down approcah:** In this approach a bulk material is broken into smaller pieces using chemical, mechanical or any other form of energy. There are so many methods which are in use for this approach and we can collectively name them as "Lithography". This technique has derived from the semiconductor industry and these lithographic techniques have made us to have a material in nano range. Some of the techniques are as under Photolithography, Scanning Lithography, Soft Lithography, Nano contact printing etc.
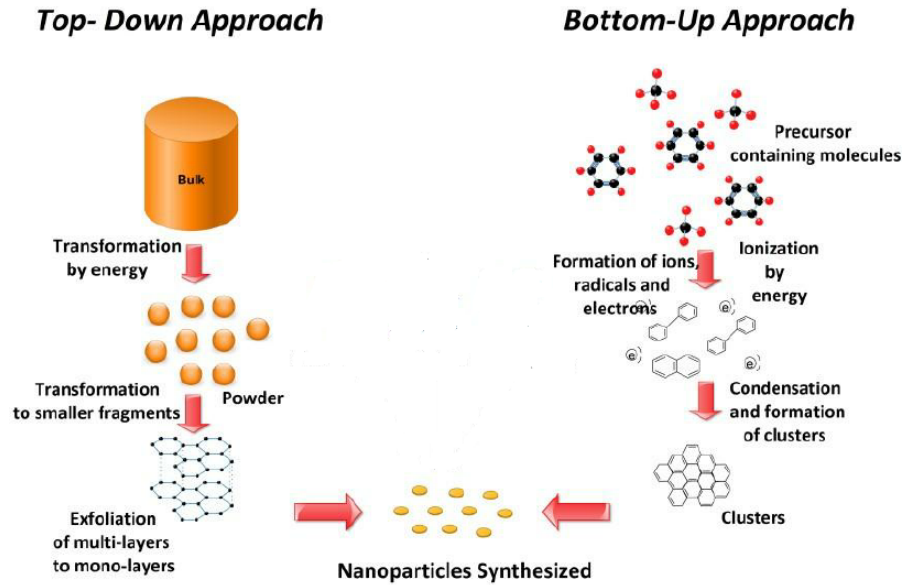
Figure 1.9: Nanomaterial synthesis approaches [23]

- **Bottom-up approcah:** In this approach nanomaterials are synthesized from atomic or molecular species via chemical reactions or self-assembly. In this way the precursor particles are allowed to grow in size or gradually assemble until desired structure is achieved. The bottom up approach can be sub divided in two phases; gas and liquid. Gas phase includes plasma arcing and vapor deposition while the liquid phase bottom up approach includes sol gel synthesis and molecular self assembly.

Both approaches require control on fabrication conditions (e.g. control on electron beam energy) and control on environmrntal conditions (e.g. extremely clean surroundings). Given the requisites are met, most important aspects contributing to the efficiency of any method lies in the capability of controlling:

- particle size

- particle shape

- size distribution

- particle composition

- degree of particle agglomeration

Table 1.2 categorizes various synthesis methods according to approaches on which they are based.

Top-down approcah	Bottom-up approcah
Milling	Vapor-phase techniques
Electro-explosion	Deposition techniques
Lithography	Chemical vapour condensation
Sputtering	Chemical reduction
Laser ablation	Sol-gel
Aerosol-based techniques	Precipitation

Table 1.2: Nanomaterial synthesis methods and respective basis approaches

Chapter 2

Literature Review

2.1   Ferrites

Ferrites (at nano-scale) come under the class of extensively studied nanomaterials. Ferrites form a big class of oxides with outstanding magnetic properties [26, 27]. Nowadays, nanoferrites have gained interest of researchers due to their significance in science and large number of applications in industry and technology [28, 29]. Ferrites are studied due to their special properties in cermaics and manetic devices [26]. These ceramic magnets have been regarded as important electrical and electronics engineering materials for the last 60 years [30]. Ferrites being the ceramic like ferromagnetic materials are basically composed of ferric oxide. The saturation magnetization of ferrites is less than ferromagnetic alloys but they have many advantages. Ferrites show significant contributions in many fields including applicability at higher frequencies, economical price, greater heat resistance and enhanced corrosion resistance. In dehydrogenation reactions, the ferrites are used as catalysts [31]. Applications of ferrites are based on their specific properties of higher electrical resistivity, lower electrical losses and good chemical stability [27]. Synthesizing ferrites at nano scale has opened up an exciting research field with remarkable applications in the electronic world. The ferrites have certain advantages over other magnetic materials. Important magnetic materials like iron and metallic alloys possess low electrical resistivity which makes them inefficient for use at higher frequencies. As ferrites exhibit high electrical resistivity, they behave well at higher frequencies. Moreover, ferrites have temperature stability and possess high permeability which have enhanced their use in high frequency electronics. Additionally, ferrites are usually economical as compared to magnetic metals and alloys. Ferrites show flexibility in the magnetic and mechanical parameters as compared to any other magnetic material [32].

2.2 Hard and Soft Ferrites

Ferrites are divided into two types, soft and hard ferrites, based on their ability to be magnetized and demagnetized. Soft materials are easy to magnetize and demagnetize, so can be used for electromagnets, whereas hard materials are used for permanent magnets because of their high coercivety. An object under the influence of applied magnetic field gets saturated and a maximum magnetization is attained, which is not increased by the application of larger field, such magnetization is called the saturation magnetization. When the applied field is reversed, the magnetization will be reduced to zero at a certain point, but then it will go to the maximum value of magnetization in the opposite direction. However, in ferromagnetic materials, the magnetization does not pass through the origin, hence a symmetric ferroic M-H loop is formed ('M' is the magnetization and 'H' is the applied magnetic field). Such materials will retain certain value of magnetization because the M-H loop does not go through the origin even when the applied field is at zero, this value of magnetization is termed as remnant magnetization. The value of the magnetic field that is to be applied in the opposite direction to force the remnant magnetization back to zero is known as coercivity. In other words, coercivity is the measure of applied magnetic field when the M-H loop crosses the zero magnetization. The magnetic materials are divided into two different categories; hard and soft. This division is on the basis of the ability of magnetic materials to get magnetized and demagnetized. The magnetic materials can also be grouped according to the strength of their coercive fields.

Hard ferrites are the ferrites exhibiting high coercivity. Generally, the values of remnant magnetization are higher for hard ferrites. The values of remnant magnetization reach up to 50% of the saturation magnetization in randomly oriented objects. Whereas the remnant magnetization can be increased up to 100% of the saturation magnetization in objects having well oriented domains. In this state, a widespread square looking M-H loop can be observed. Hard ferrite magnets are used to make magnetic arrangements of two types:

- **Isotropic** magnets are formed to preferred shapes, sintered and then magnetized which exhibit magnetic fields of moderate strength and have applications in ring magnets and cycle turbines.

- **Oriented** magnets are aimed to form under a strong magnetic field and then sintered which exhibit a very strong magnetic field and used in magnets of two wheelers like bikes, loudspeakers [33].

Soft ferrites are the ferrites having low coercivity. Only small magnetic field application is required by the soft ferrites to minimize the magnetization to zero. As a

13

consequence, the values of remnant magnetization are smaller as the magnetization is already going to zero when the applied magnetic field is zero. Hence, contracted M-H loops are formed by the soft ferrites. Soft ferrites are also semiconductors, indicating that they are somewhere between insulators and conductors based on their ability to conduct electron flow through the material. These two types of ferrites have different important applications [34].

2.3 Magnetism and its Classification

Magnetism in materials is based on the manner in which they respond to an applied field. Different types of magnetism are identified according to the orientations of magnetic moments in materials. There are five main classes of magnetism, namely; diamagnetism, paramagnetism, ferromagnetism, anti-ferromagnetism and ferrimagnetism. Magnetic ordering rises as a result of the alignment of the unpaired electronic spins on nearby atoms through the exchange interactions. When a magnetic field is applied through any source to a material, the atomic currents generated by the circular movement of electrons respond to the applied field. In each type of magnetism this response is different. Different magnetic behaviours are depicted in Figure 2.1.
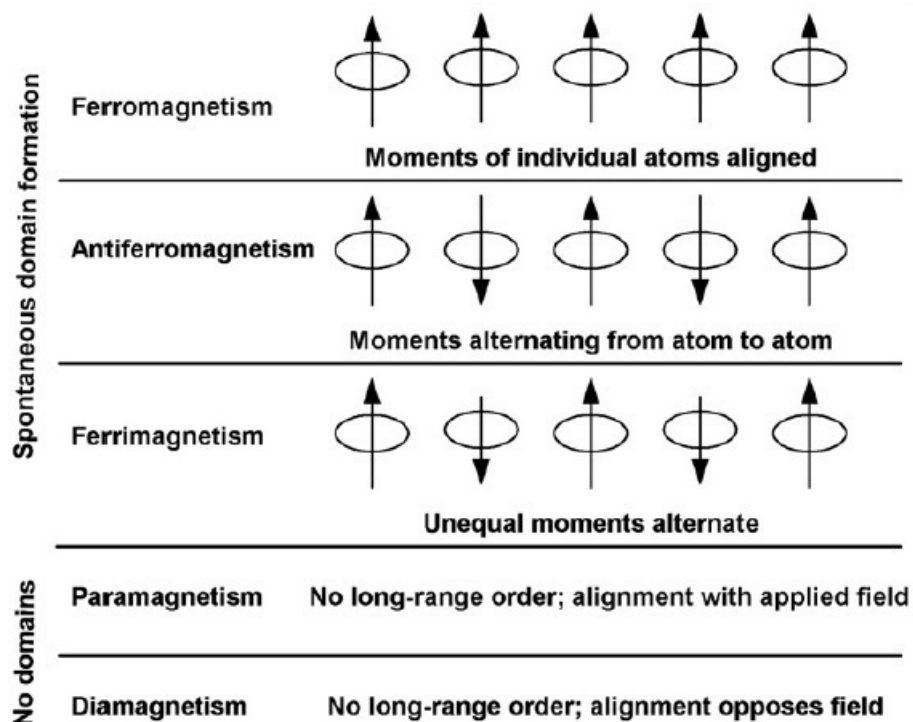
Figure 2.1: Different types of magnetic behaviour [32]

2.3.1 Diamagnetism

In diamagnetism when a magnetic field is applied, atomic currents (circular movement of electrons) respond in opposition to the applied field. This kind of weak repulsion is depicted by all materials. Diamagnetism is very weak. Materials having their electron sub-shells full, exhibit diamagnetism. Pairing of moments in diamangets occurs in such a way that they nullify each others' effect. Materials exhibiting diamagnetism show weak repulsion to applied fields. The susceptibility of such materials is negative ($\chi < 0$).

2.3.2 Paramagnetism

Materials having unpaired magnetic moments exhibit paramagnetism. The effect of ordering of moments is not long-range in substances possessing paramagnetic properties. The susceptibility in these materials is positive but almost zero ($\chi \approx 0$).

2.3.3 Ferromagnetism

Ferromagnetism occurs when equi-magnitude moments are in alignment. Without applying an external field, spontaneous magnetization can occur in ferromagnetism. Figure 2.1 depicts ferromagnetic behaviour.

2.3.4 Antiferromagnetism

Anti-parallel alignment of equi-magnitude moments is exhibited by antiferromagnetic materials. Hence, the net magnetization is zero. An example of antiferromagnetism is found in MnO.

2.3.5 Ferrimagnetism

Alignment in ferrimagnetic materials is similar to antiferromagnetic materials, other than the fact that opposing moments are unequal. Therefore, spontaneous magnetization is observed [32]. Ferrimagnetic ordering is shown in Figure 2.1.

2.4 Ferrites on Basis of Structures

Ferrites exist in three different structural configurations namely; garnets, hexagonal and spinel ferrites. This classification of ferrites is on the basis of their sizes and charge on the metal ions which is compensated by the charge on oxygen ions and their relative compositions [35]. Among these three distinct ferrites, special attention would be towards spinel ferrites because mostly the important ferrites have spinel structural

symmetry. Spinel ferrites are regarded as one of the two important inorganic nano-materials due to their optical, magnetic, catalytic and electrical properties [36, 37].

2.4.1 Garnets

The ferrite garnets are represented by the general formula $R_3Fe_5O_{12}$. R stands for the rare earth trivalent cations including Y, La and Gd. Ferrimagnetic garnets show iso-morphism with the naturally occurring garnet $Ca_3Fe_2(SiO_4)_3$ [38]. The crystal structure exhibits cubic symmetry and is complicated comparatively. The unit cell of the cubic structure is formed by 8 formula units which contain 160 atoms making a special arrangement including 96 oxygen ions with the interstitial cations. $Y_3Fe_5O_{12}$ (YIG) is a known garnet named as Yttrium iron garnet. These garnets were prepared by Bertaut and Forrat in 1956 for the first time and their detailed study was done by Geller and Gilleo in 1957 [27]. A closely packed arrangement is absent and the structure can be regarded as an oxygen polyhedra combination. The O polyhedra describes three cation sites, the eight-fold dodecahedral, the six-fold octahedral and the four fold tetrahedral. The dodecahedral sites are occupied by the rare-earth ions and the octahedral and tetra-hedral sites are occupied by the Fe cations. There are 24 dodecahedral, 16 octahedral and 24 tetrahedral sites. The polyhedral combination is shown in Figure 2.2.
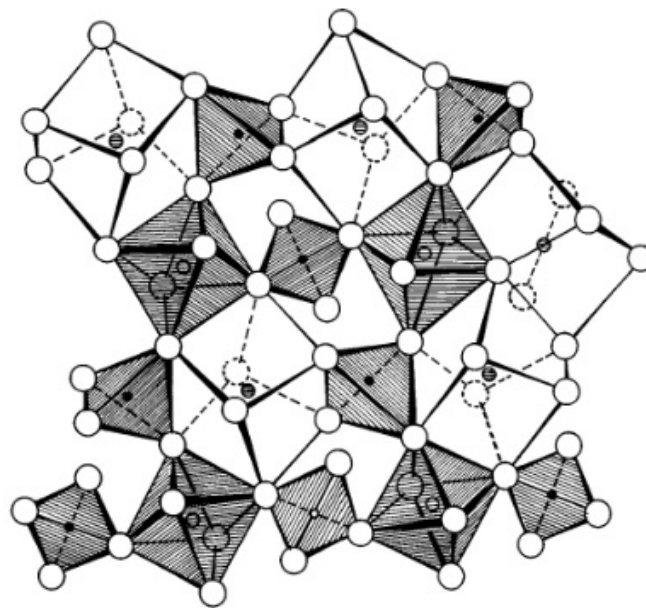
Figure 2.2: Garnet structure described as a ployhedra structure [27]

A large number of transition metal ions can replace the cations present in the garnet structure. Other metal ions could be accepted by the three dodecahedral, octahedral and tetrahedral lattice sites [27, 37, 39].

2.4.2   Hexagonal Ferrites

Hexagonal ferrites are categorized by their high coercivity and are used as permanent magnets [40]. These ferrites are represented by the general formula of $MeO.6Fe_2O_3$. Me could be Ba, Sr, or Pb [41]. The crystal structure of hexagonal ferrites resembles to the mineral magnetoplumbite [34, 38]. With closely packed oxygen ions, hexagonal and spinel ferries have same structures, but few layers contain metal ions. The ionic radii of the metal ions is nearly the same as that of the oxygen ions. The metal ions can reside on the three tetrahedral, octahedral and trigonal bi pyramid lattice sites enclosed by oxygen ions [37].

2.4.3   Spinel Ferrites

Spinel ferrites can be regarded as the most important family of ferrites. Spinel ferrites are recognized as one of the most important magnetic materials due to their wide range applications [42,42]. Spinel ferrites can be represented by the general formula MFe_2O_4 (M is a metal cation). Synthesis and characterization of spinel ferrites at nano scale has gained attention [44–49]. The properties of the spinel ferrites are effected by the parameters used during their synthesis, which govern two significant characteristics that are the particle sizes and the sub-lattice division of cations [50].

2.4.3.1   Structure of Spinel Ferrites

The spinel ferrites has general formula of AB_2O_4 where A represents a divalent metal ion such as magnesium, iron, nickel, manganese and zinc. The B represents trivalent metal ions such as aluminum, iron, chromium and manganese. However, titanium Ti^{4+} and Pb^{2+} etc. may also occupy this site. In most oxide structures, the oxygen ions are appreciably larger than the metallic ions and the spinel structure can be approximated by a cubic close packing of O^{2-} ions in which the cations (e.g. Co^{2+}, Fe^{3+}) occupy certain interstices.
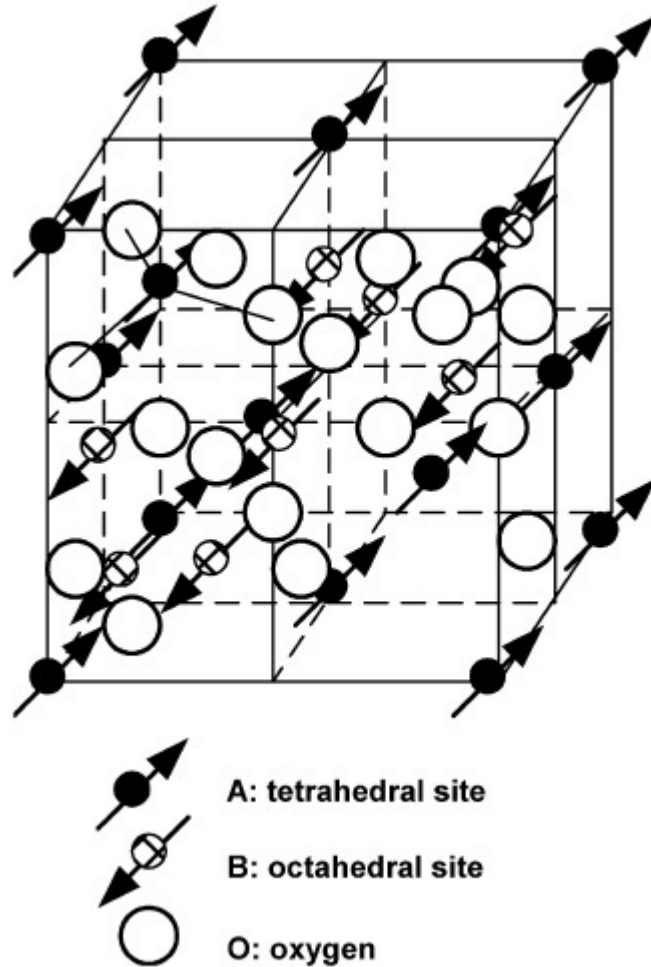
Figure 2.3: Schematic of a partial unit cell and ferrimagnetic ordering of spinel ferrite structure [32]

The position of the A ions is nearly identical to the positions occupied by carbon atoms in the diamond structure as the structure of a spinel compound is similar to the highly symmetric structure of diamond. This can explain the relatively high hardness and high density typical of this group. The arrangement of the ions also favors the octahedral crystal structure, which is the predominant crystal form and is in fact the trademark of the spinels. There are well over a hundred compounds with the spinel structure reported to date. Most are oxides, some are sulphides, selenides and tellurides and few are halides. Many different cations may be introduced into the spinel structure and several different charge combinations are possible.

In oxide spinels, the two types of cations do not usually differ greatly in size, because the spinel structure is stable only if the cations are rather medium sized and, in addition, the radii of the different ionic species in the same compound do not differ too much. Similar cation combinations occur in sulphides, e.g. $Zn^{2+}Al_2^{3+}S_4$ and $Cu_2^{2+}Sn^{4+}S_4$. However, in halide spinels e.g. $Li_2^{1+}Ni^{3+}F_4$ and $Li^{1+}Mn_2^{3+/4+}F_4$, cations

are limited to charges of +1 and +2, in order to give an overall cation: anion ratio of 3:4. Most spinels fall into three series determined by a B metal: aluminate series with Al^{3+} (Hercynite, Gahnite, Galaxite); a magnetite series with Fe^{3+} (Magnetite, Magnesio ferrite, Franklinite); a chromite series with Cr^{3+} (Chromite, Magnesio, chromite). There is extensive cationic exchange (solid solution) within each series but very little between the series.

The structure of spinel ferrites can be viewed as closely packed face centered cubic arrangement of oxygen atoms in which 32 ions of oxygen form a unit cell. The layers of the oxygen ions consist of 64 tetrahedral (A) and 32 octahedral (B) sites. The structure of a spinel has two cation sites for the occupancy of metal cations. There are eight A sites in which the metal cations are coordinated with oxygen tetrahedrally and 16 B sites which have octahedral coordination with oxygen ions.

Depending upon the distribution of metal and iron cations in the two crystallographic sites, the spinel ferrites can exist as normal, inverse or mixed spinels. The division of divalent and trivalent cations among the tetrahedral and octahedral sites can be represented by the formula $(M_\delta Fe_{1-\delta})\,[M_{1-\delta}Fe_{1+\delta}]O_4$, where M represents a divalent cation and δ is the inversion degree.

- **Normal Spinels:** In a normal spinel, the A-sites are occupied by the metal cations and the B-sites are occupied by the Fe^{3+} cations. The cation disorder is defined in terms of a "normal" spinel structure, such as that for ideal $MgAl_2O_4$, in which all the Mg resides on sites tetrahedrally coordinated with oxygen, and all the Al resides on sites octahedrally coordinated with oxygen. Normal spinel
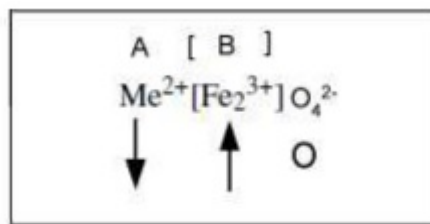
Figure 2.4: Cation distribution in normal spinel [32]

structures are usually cubic closed-packed oxides with one octahedral and two tetrahedral sites per oxide. The inversion parameter is defined relative to this configuration, and is the ratio of the atomic fraction of Al on tetrahedral sites to the atomic fraction of Al on octahedral sites. The tetrahedral points are smaller than the octahedral points. B3+ ions occupy the octahedral holes because of a charge factor, but can only occupy half of the octahedral holes. A^{2+} ions occupy

1/8th of the tetrahedral holes. This maximizes the lattice energy if the ions are similar in size. Zinc ferrites come under the category of normal spinel ferrites.

- **Inverse Spinels:** In the structure of an inverse spinel, the divalent metal cations occupy the octahedral sites and the trivalent iron cations are distributed among the tetrahedral and octahedral sites. For an ideal "inverse" spinel structure (such as for $MgFe_2O_4$), all of the Mg resides on octahedral sites, and the Fe is distributed equally over the remaining octahedral sites and all of the tetrahedral sites. In this case the inversion parameter would be 1.0. If the A^{2+} ions have a strong preference for the octahedral site, they will force their way into it and displace half of the B^{3+} ions from the octahedral sites to the tetrahedral sites. If the B^{3+} ions have a low or zero octahedral site stabilization energy, then they have no preference and will adopt the tetrahedral site. A common example of an inverse spinel is Fe_3O_4. Magnetite, nickel ferrites and cobalt ferrites have inverse spinel structures.
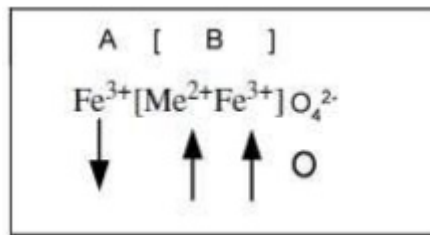
Figure 2.5: Cation distribution in inverse spinel [32]

- **Mixed Spinels:** The A and B sites are occupied by divalent metal and trivalent iron cations respectively in the structure of a mixed spinel ferrite. Manganese ferrites are an example of mixed spinel ferrites [32,51].
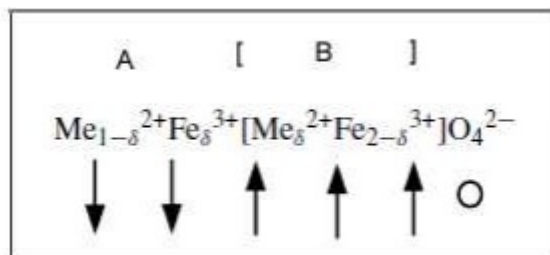
Figure 2.6: Cation distribution in a mixed spinel [32]

2.4.3.2 Applications of Spinel Ferrites

Spinel ferrites have gained noticeable consideration in recent years due to their applications in [52–62]:

- Electronic devices

- High density information storage media

- Drug delivery

- Radio frequency circuits

- Rod antennas

2.4.3.3 Magnetic Properties of Spinel Ferrites

Neel explained that the magnetic moments of ferrites are the resultant of the individual magnetic moments of the sub-lattices. In spinel ferrites, these sub-lattices are A and B. The sub-lattice A contains the cations at the tetrahedral positions and the sub-lattice B consists of cations at the octahedral positions. There are different values of exchange interaction between the electrons of the ions in the A and B sites. The interaction between the magnetic ions of sub-lattices A and B that is the A-B interaction is the strongest generally. The A-A interaction is nearly ten times weaker and the B-B interactions are the weakest of all. The main A-B interactions give way towards the complete or partial anti ferromagnetism. In inverse spinel ferrites, half of the trivalent iron cations are positioned at the A-sites and another half at the B-sites. Their magnetic moments are balanced by each other and the resultant magnetic moments of the inverse spinel ferrites is because of the magnetic moments of divalent cations residing at the B-sites [63].

2.5 Magnesium Ferrites

Magnesium ferrites ($MgFe_2O_4$) have gained special consideration among other ferrites due to their wide range applications in high density recording media, sensors and magnetic technologies. Their wide range utility and importance is mainly attributed to the interesting magnetic and electrical properties they posses with thermal and chemical stability. Magnesium ferrites are soft, magnetic semiconducting materials. General properties of magnesium ferrites are tabulated in Table 2.1 [64].

Property	Type
Crystalline structure	Cubic
Spinel type	Normal spinel
Semiconducting material	n-type

Table 2.1: General properties of magnesium ferrites

Chapter 3

Characterization Techniques and Experiments

3.1   Experimental Work

Practical work performed to accomplish this study comprises the following tasks:

- Synthesis of nickel doped magnesium ferrites

- Pellets fabrication

- Analysis of dielectric and gas sensing properties of fabricated pellets

- Analysis of structural and morphological properties of powdered samples

Equipment used

Following are the apparatus and techniques used for the samples preparation.

- Magnetic hot plate

- Digital weight balance

- Drying oven

- Muffle furnace

- Mortar and Pestle

- China Dish

- Die

- Hydraulic press

Magnetic Hot Plate

Magnetic hot plate with magnetic stirring was used to sustain the temperature of chemical reaction.

Digital Weight Balance

Digital electronic weight balance is the main tool used in nano synthesis laboratory for accurate measurements of chemical weight.

Drying Oven

Drying oven was used for the evaporation of solvent.

Muffle Furnace

Muffle furnace was used for heating of samples at higher temperature.

Mortar and Pestle

It was used for crushing and grinding of obtained samples and transforming it into finer form for structural and morphological analysis.

Die

For dielectric and electrical properties it was necessary to transform the material into pellet form.

Hydraulic press

Hydraulic press is instrument that was used for the pellets formation in die. By compressive forces it can make the solid powder in compact pellet form.

3.1.1 Nanoparticles' Synthesis by Co-precipitation

$Mg_{1-x}Ni_xFe_2O_4$ ($x = 0.0, 0.2, 0.35, 0.5$) nanoparticles were synthesized through wet chemical co-precipitation route. The co-precipitation method is based on the bottom-up synthesis approach. General steps involved in this method are illustrated in Figure **??**. However, specific conditions are required for each synthesis for example specific precursor reactions. To attain desired properties of synthesized nanoparticles, close monitoring and control on pH, concentration, temperature and stirring speed of the mixture are essential. The chemicals of

- magnesium nitrate [$Mg(NO_3)_2.6H_2O$],

- nickel nitrate [$Ni(NO_3)_3.6H_2O$],

- iron nitrate [$Fe(NO_3)_3.9H_2O$] and

- sodium hydroxide [$NaOH$]

were used in the preparation of Mg/Ni ferrites. Solutions of magnesium nitrate, nickel nitrate and iron nitrate were made separately using deionized water as a solvent followed by constant stirring at room temperature. The three solutions were then mixed in a beaker and further magnetic stirring was carried. The mixture of solutions was heated and the temperature was maintained at $90\,°C$. 3M solution of sodium hydroxide was also prepared and heated at $90\,°C$. Solution of sodium hydroxide was added in the solution of nitrates and the temperature was maintained at 90°C for 45 minutes. The solution was then allowed to cool at room temperature and stirring was continued. Washing was done

7 times and the precipitates were allowed to settle down in the beaker. Overnight drying of precipitates was carried out in the oven at $100\,^{\circ}$C. The ferrite nanoparticles were then grinded to powder form using the mortar and pestle. The powder was then calcined at $800\,^{\circ}$C in the muffle furnace for 8 hours. After calcination, fine grinding of all the samples was performed. 1 gram powder of each sample was used to make pellets using the hydraulic press. 5 tons of pressure was applied to powdered nanoparticles for four minutes. Specac Die (Britan) was used in the preperation of pellets. Pictorial representation of the synthesis process is given in Figure 3.1.
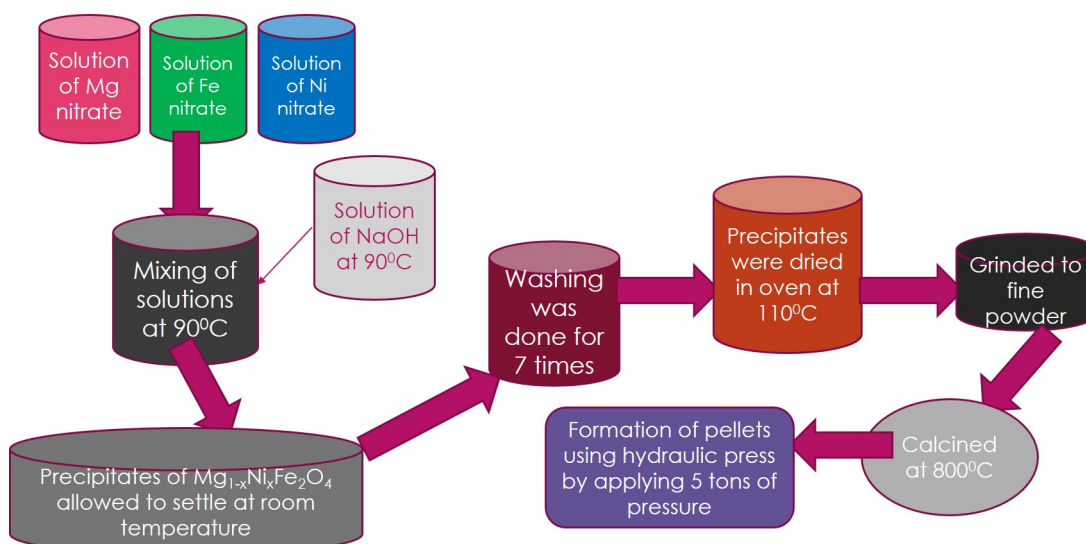
Figure 3.1: Ferrite samples' synthesis flow chart

In this research work, the crystal structure was examined through XRD analysis, using STOE Germany X-ray Diffractometer, operated at Theta-Theta mode, with emission source of Cu K having wavelength of 1.54 Å. The spinel phase formation was further observed by Fourier Transform Infrared (FTIR) spectra, using the Perklin Elmer spectrum FTIR spectrometer. The JEOL JSM-6390 Scanning Electron Microscopy (SEM) was utilized for analyzing the surface morphology of the prepared ferrites. The dielectric properties were studied with the help of Wayne Kerr LCR 6500B.

3.1.2 Gas Sensing Test Setup

The sensing of nitrogen, oxygen and methane gases by the synthesized ferrites was examined using a specifically designed sensing chamber. A sample holder was placed inside the chamber and the pellet was inserted into the sample holder. The holder was connected to a multimeter. A constant voltage was supplied to the sensing materials and the flowing current was measured using an ammeter, then resistance was calculated. Firstly, the resistance of the sample was measured using the multimeter in the absence of gas. The gases were then allowed to enter the glass chamber from the inlet valve one by one using a syringe. Then resistance of the samples was measured in the presence of gas. Sensitivity was calculated using the values of measured resistances [66]. After making measurements, gas was allowed to move out with the help of an outlet valve at the opposite wall of the chamber. Once the sensor element was exposed to a gas, it was subjected to heat treatment to remove any impurities before taking a new measurement [67]. Sensitivity is measured by Equation 3.1. Setup used for gas sensing is illustrated in Figure 3.2.

$$S = \frac{|R_a - R_g|}{R_a} \times 100 \qquad (3.1)$$
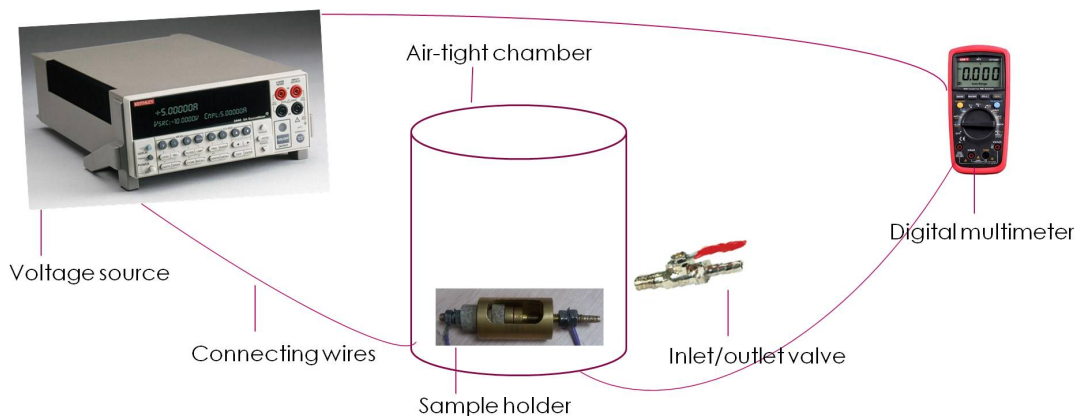
Figure 3.2: Gas sensing setup

3.2 Characterization Techniques

In comparison to bulk materials, nanomaterials may exhibit changes in their properties or even in some cases additional properties, mainly due to their increased surface-to-volume ratio and quantum effects. In order to ascertain these modified properties, it is essential to characterize nanomaterials. Nanomaterials are generally characterized by the following parameters [1]:

- Shape, size of particles, aspect ratio

- Degree of aggregation and agglomeration

- Size distribution

- Specific surface

- Surface chemistry

- Crystal structure

- Surface modification

A variety of techniques are used for characterization of nanomaterials. These various techniques are drawn from interdisciplinary areas. Most commonly used characterization techniques are provided in Table 3.1 [1].

Techniques	Characterization Parameters
DLS	Size
	Size distribution
SEM	Shape
	Surface structure
TEM	Size, shape
	Morphology
AFM	Shape
	Surface morphology
STM	Surface images
	Modification of material
LSCM	Migration of nanoparticles
	3D morphology
BET	Surface area analysis
	Porosity
	Adsorption capability
FTIR	Assisted analytical tool for chemical composition
DSC	Thermal analysis
	Phase transitions

Table 3.1: Common characterization techniques

3.3 Characterization Techniques Used

Several techniques of characterizations were used to analyze the properties of the samples prepared; these are mentioned below.

3.3.1 XRD

X-ray diffractometry (XRD) at high resolution is an appropriate way to identify the crystal structures. As the wavelength of X-rays is similar to the inter-atomic spacing, their usage has become significant. Monochromatic beam that is of one wavelength is required mostly. XRD finds out what is happening when x-rays are incident on a material and the rays being diffracted. The scattered rays spread out in all the directions and are visualized at different angles. Typically, an X-ray spectrum consists of a number of wavelengths. A continuous X-ray spectrum is obtained for every accelerated potential. X-ray diffractometer gives us informa-

tion about the nature of the crystal without causing any destruction to the sample [68–70].

X-ray diffractometer is basically the practical implementation of Bragg's Law. Bragg's Law explains conditions in which these X-rays can diffract and interfere through the crystal structure which is governed by the relation:

$$2d \sin \theta = n\lambda \tag{3.2}$$

d = inter-atomic spacing
θ = diffraction angle
λ = source wavelength
Schematic of Bragg's Law is shown in Figure 3.3 [71].
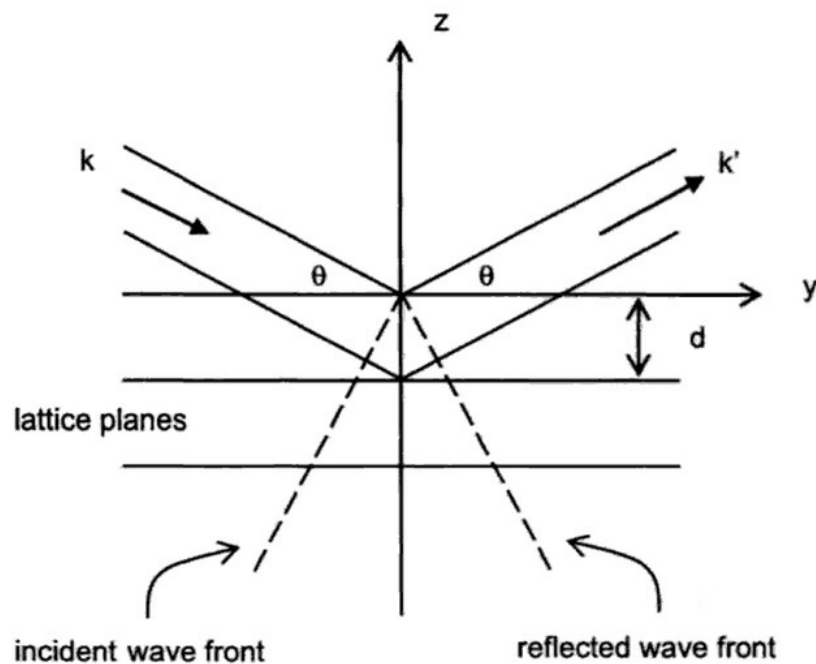

Figure 3.3: X-ray diffraction (Bragg's Law) [71]

Provided the diffraction angle (θ) is known, crystallite size (D) of a material can be estimated using the Debye Scherer's equation:

$$D = \frac{0.9\lambda}{\beta \cos \theta} \tag{3.3}$$

0.9 = crystal shape factor

λ = source wavelength

θ = diffraction angle

β = full width at half maximum

Lattice parameter (a) is estimated using the relation [72]

$$a = d\sqrt{h^2 + k^2 + l^2} \tag{3.4}$$

d = inter-atomic spacing

h, k, l = miller indices

X-ray density (ρ_x) and mass density (ρ_m) are calculated using the lattice constant

$$\rho_x = \frac{8 \times M}{N_A \times a^3} \tag{3.5}$$

$$\rho_m = \frac{m}{V} \tag{3.6}$$

M = molecular weight

N_A = Avogadro number

m = sample mass

V = pellet volume

Porosity (P) is measured using X-ray density and mass density

$$P = 1 - \frac{\rho_x}{\rho_m} \tag{3.7}$$

3.3.2 Scanning Electron Microscope (SEM)

Scanning electron microscopy is used for studying the surface morphology at the nanoscale dimensions. Sample preparations of SEM don't re-

quire a complex process. The surface of the sample must be conductive so non-conductive materials must be coated with thin metallic surface.

The SEM uses a beam of high-energy electrons that produces a high resolution image. A beam of electrons travels through electromagnetic fields and lenses and hits the sample. Due to interactions of incident electrons and the sample, electrons and X-rays are ejected from the sample. Figure 3.4 illustrates the phenomenon. Internal structure and working of a typical SEM is depicted in Figure 3.5.
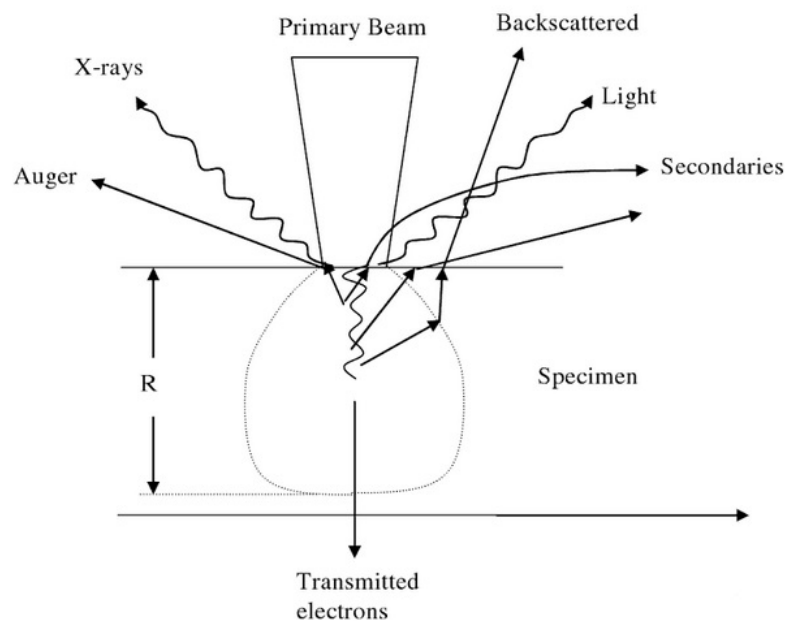
Figure 3.4: Signals derived from electron-sample interactions in SEM [73]

The main constituents of SEM are discussed below:

Electron Gun

Electron gun in SEM is made by using tungsten filament .When electric current pass through the tungsten filament electrons are generated. Anode is placed near the filament to attract the electrons. But electrons are not following the well orientated path, for this reason cathode is also placed near to the filament that repels the electrons. The electronic cloud is attracted to the anode plate to the cathode plate through hole.

Figure 3.5: Schematic of SEM [73]

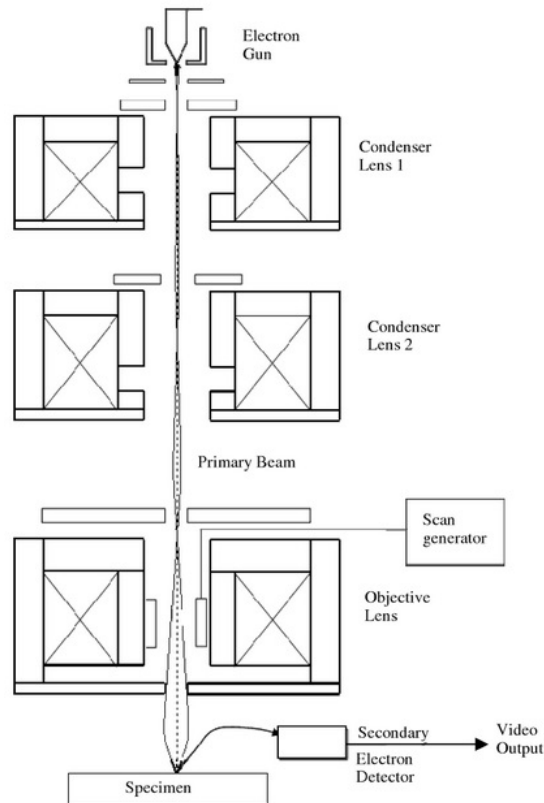The emission speed of the electrons from the electron gun is organized by accelerating voltage that is applied to the cathode and anode plates.

Electromagnetic Lenses

A beam of electrons from electron gun is controlled by the electromagnetic lenses. The construction of magnetic lenses consists of a wire coiled around an iron cylindrical core. By passing electric current through a wire magnetic field is generated which acts as a magnetic lens. These magnetic lenses and electron gun in sample chamber are arranged in such a way that condenser lenses control the size of the beam. Beam is focused on the sample by objective lenses. The benefit of electromagnetic lenses over the glass lenses is that focal length of electromagnetic lenses is adjustable by changing the current through the wire. There are so many modes in which SEM can operate. The selection of operating mode depends upon the sample and features we need to study. The two

modes are briefly explained here.

Secondary Electrons

When the incident beam electrons hits a sample atom electrons, ionizes the atoms and knock it out of its outermost shell. These are the secondary electrons. Secondary imaging mode reveals the information about the surface topography. Secondary electrons provide morphological and topographic information of samples.

Backscattered Electrons

When the incident beam strikes with the nucleus of the sample atom backscattered electrons are produced. Backscattered electrons are related to the atomic number and density of the sample surface. A sample surface with greater atomic weight area scatters more backscattered electrons as compare to the low atomic weight area. Contrasts in composition of samples are estimated on basis of data provided by backscattered electrons. Typical energy spectrum of electrons leaving the specimen is given in Figure 3.6.
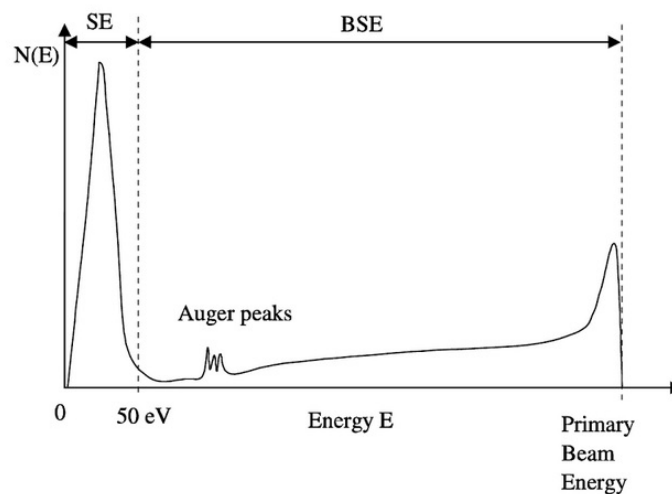

Figure 3.6: Energy spectrum of electrons leaving the specimen [73]

3.3.3   FTIR Spectroscopy

In general, the fourier transform infrared (FTIR) spectroscopy is a technique used to obtain an infrared spectrum of absorption or emission of a material sample. FTIR is also commonly applied to gather information regarding vibrations of metal-oxygen bonds in an under test sample. An FTIR spectrometer simultaneously collects high spectral resolution data over a wide spectral range [74].

In the FTIR device, (Figure 3.7) light beam from a polychromatic infrared source is collimated and directed to a beam splitter. In ideal circumstances, 50% of the light reaches the moving mirror, while the remaining light is refracted to the fixed mirror. Both mirrors, reflect light back to the beam splitter and a certain fraction of the original light passes into the sample compartment. Here, the light focuses on the sample. The light is refocused on to the detector upon leaving the sample compartment. The difference in optical path length between the two paths is known as retardation. Output spectrum data points are obtained by varying the retardation, and recording the signal from the detector for various values of the retardation.

Analysis made on basis of FTIR output data uses, the peak position, the peak width, and the peak intensity. Materials' identification is primarily based on the peak position.
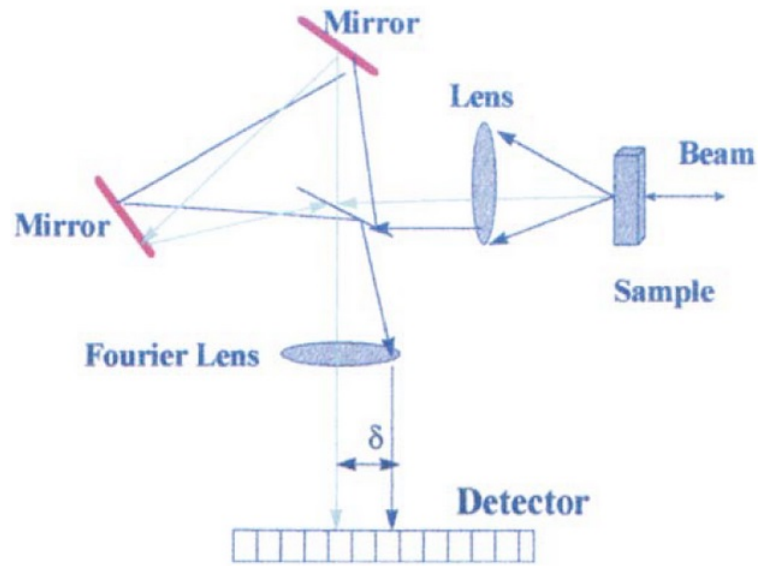
Figure 3.7: Functional schematic of a typical FTIR device [74]

3.3.4 Dielectric Characterization

For dielectric characterization, the following attributes of samples are analyzed.

3.3.4.1 Dielectric constant

Dielectric constant is calculated using relation 3.8.

$$\varepsilon' = \frac{\varepsilon^\circ \times D}{C \times A} \qquad (3.8)$$

3.3.4.2 Dielectric Loss

Dielectric loss is calculated using relation 3.9.

$$\varepsilon'' = \varepsilon' \times D \qquad (3.9)$$

3.3.4.3 Tangent Loss

Tangent Loss is calculated using relation 3.10.

$$\delta = \frac{\varepsilon''}{\varepsilon'} \qquad (3.10)$$

3.3.4.4 AC Conductivity

AC conductivity is calculated using relation 3.11.

$$\sigma = 2\pi f \varepsilon^{\circ} \varepsilon''$$
(3.11)

LCR meter is an electronic device that measures inductance, capacitance, and resistance at various frequencies with high precision and accuracy. LCR meter is used in two configurations for impedance measurement.

- **Current-voltage method:** this method is applied for analyzing dielectric properties at high frequencies. Within this method two separate measurement configurations are used for low and high impedance circuits (Figures 3.8 and 3.9).
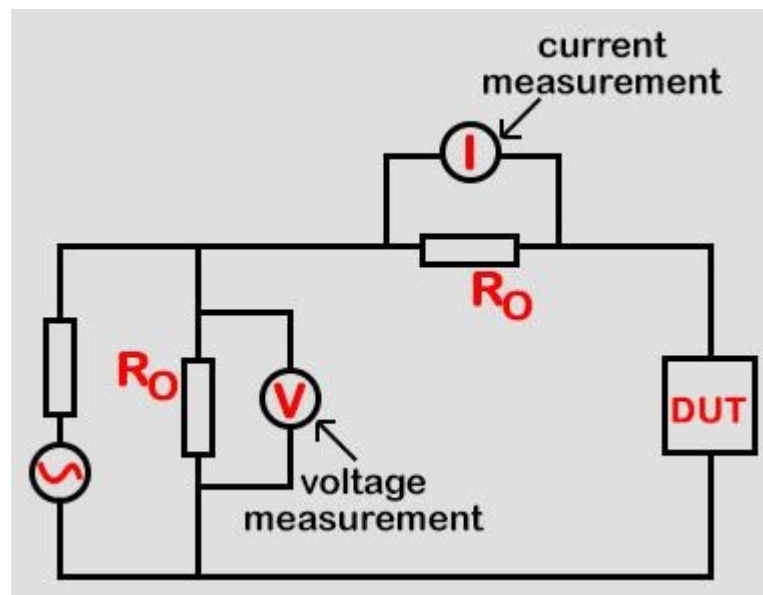

Figure 3.8: Current-voltage configuration for high impedance circuits [75]

- **Bridge method:** this method is applied for analyzing dielectric properties at low frequencies up to 100 kHz. The method is based on Wheatstone Bridge principle (Figure 3.10). Device to be tested is placed in the bridge circuit. Two impedances in the circuit are
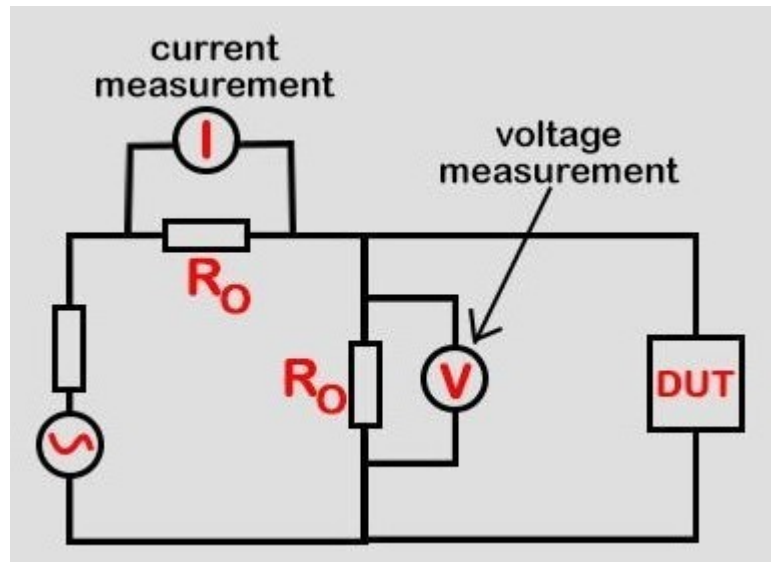
Figure 3.9: Current-voltage configuration for low impedance circuits [75]

known Z2 and Z4. When current stops flowing in the other un-
known impedance device (Z1); impedance of device under test
(DUT) is found out by the relation.
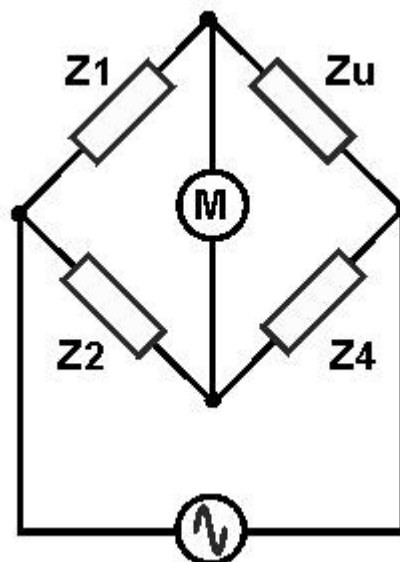
$$\frac{Z1}{Zu} = \frac{Z2}{Z4} \tag{3.12}$$

Figure 3.10: Bridge method circuit diagram [76]

Chapter 4

Results and Discussions

4.1 Structural Analysis

XRD of the powdered samples were performed to study the crystal structure. The powdered samples Nickel doped magnesium ferrites were scanned by the X-ray diffractometer in the 2θ range of $20°$ - $90°$. Diffraction patterns were obtained and indexing was processed by allotting miller indices to the intensity peaks using the software ***X'pert High-Score***. Miller indices (311) correspond to the most intense peak. Figure 4.1 shows the indexed XRD patterns of Mg/Ni ferrites at four different compositions.
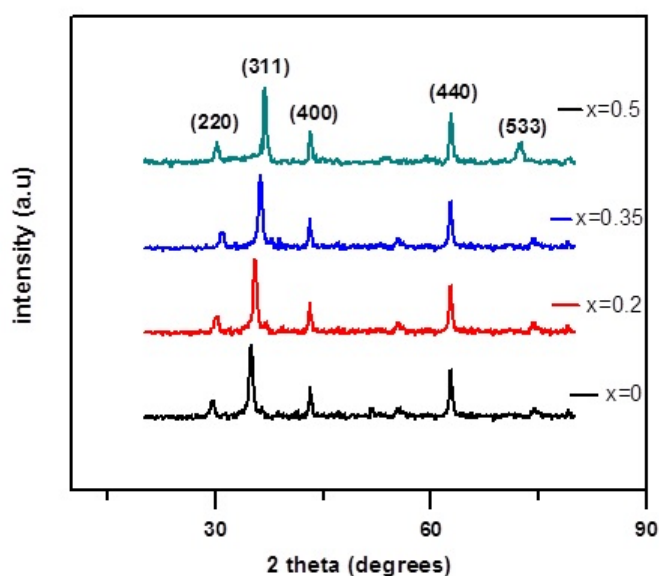

Figure 4.1: Indexed XRD patterns of $Mg_{1-x}Ni_xFe_2O_4$ with all peaks

Formation of single phase FCC spinel lattice is confirmed by the XRD pattern as no extra lines corresponding to any other crystallographic phase are observed. A shift in intense peak positions towards higher angle is noticed with increase in doping concentration as shown in Figure 4.2.
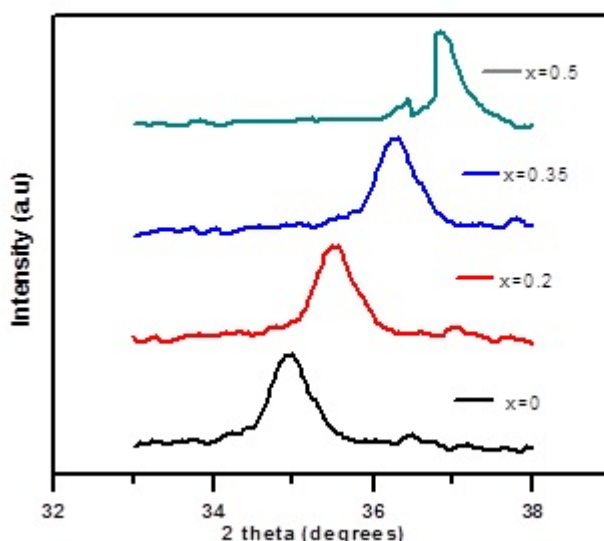

Figure 4.2: Indexed XRD patterns of $Mg_{1-x}Ni_xFe_2O_4$ with most intense peak

The inter-planar spacing d_{hkl} is estimated using the Braggs equation. The values obtained for d_{hkl} were in the range of 2.45Å-2.56Å. By using the values of d_{hkl}, the values of lattice constant 'a' were also calculated taking into account the hkl values of the most intense peaks. The lattice constants were found to be in the range of 8.32Å-8.68Å. Lattice constant for all compositions is shown in Figure 4.3.

It is observed that the lattice constant decreases with increase in Ni^{2+} ions concentration which can be ascribed to the smaller ionic radius of Ni ions as compared to Mg ions. The average crystallite sizes of all the samples were determined from the XRD peaks using the Debye Scherer's formula. Crystallite sizes acquired were in the range of 4.17 nm - 8.36 nm. The values of X-ray density, bulk density and porosity were also obtained using the equations 3.2 - 3.7. X-ray densities and mass densities for all compositions are shown in Figure 4.4.
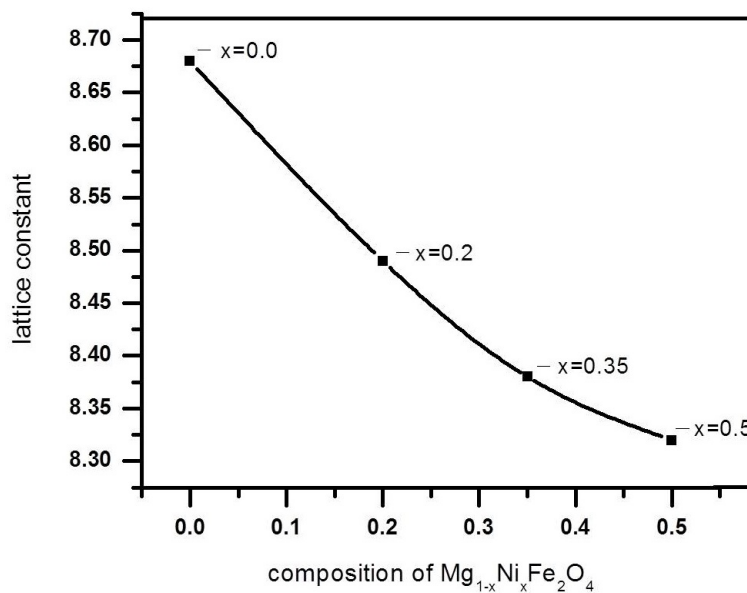
Figure 4.3: Lattice constant of $Mg_{1-x}Ni_xFe_2O_4$
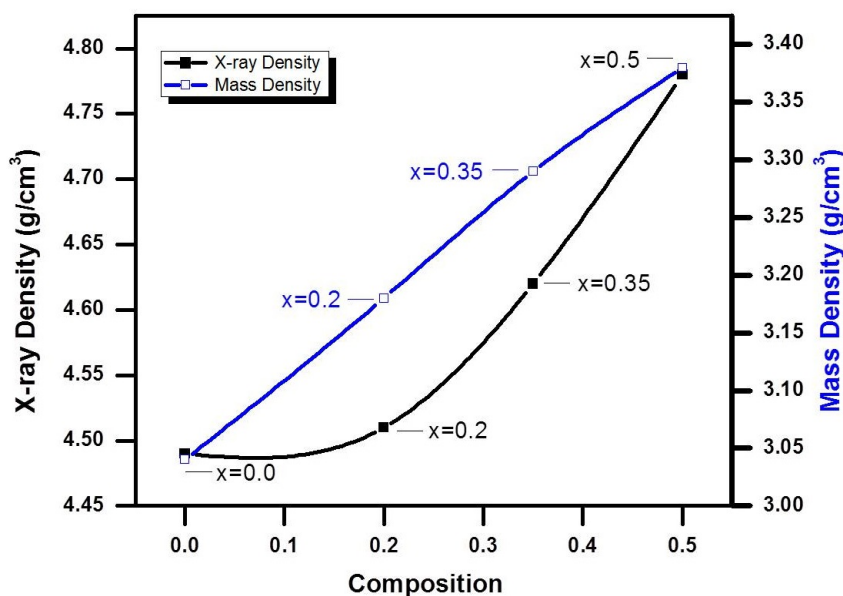
Figure 4.4: X-ray densities and mass densities of $Mg_{1-x}Ni_xFe_2O_4$

Mass density increases with increase in Ni^{2+} ions concentration, this increase can be attributed to higher atomic mass of nickel as compared to magnesium. The x-ray density also goes on increasing by increasing the quantity of dopant, this may be due to the fact that nickel has greater density as compared to magnesium. Porosity is shown in Figure 4.5.

Figure 4.5: Porosity of $Mg_{1-x}Ni_xFe_2O_4$

Porosity exhibits decreasing trend, with increase in doping content. Exact values of crystallite size, lattice constant, X-ray densities, mass densities and porosity are provided in Table 4.1.

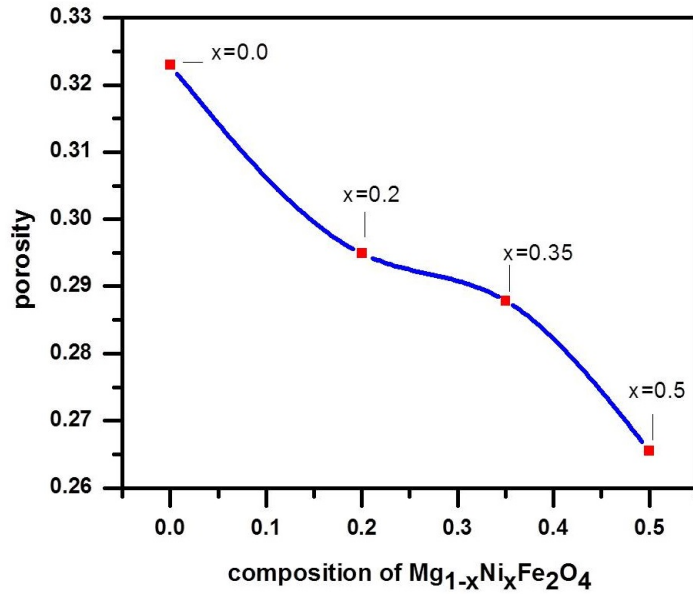| Dopant content	Crystallite Size (D) (nm)	Lattice constant (a) (Å)	X-ray density (ρ_x) (g/cm^3)	Mass density (ρ_m) (g/cm^3)	Porosity
x = 0.0	8.36	8.68	4.49	3.04	0.3229
x = 0.2	4.17	8.49	4.51	3.18	0.2949
x = 0.35	5.58	8.38	4.62	3.29	0.2878
x = 0.5	8.3	8.32	4.78	3.38	0.2655

Table 4.1: The lattice constant, X-ray density, mass density and porosity of $Mg_{1-x}Ni_xFe_2O_4$

4.2 Morphological Analysis

To determine the morphology of fabricated nanoparticles, SEM was performed. For SEM analysis, a suspension of all the finely grinded samples was prepared using deionized water by performing one hour sonication. A small droplet from each suspension was then spread on separate glass slides and exploited to a heat lamp for evaporation. To make

the samples conducting their gold plating was done using sputter coater. SEM images of all the samples are shown in Figures 4.6 - 4.9. The average particle sizes of $MgFe_2O_4$, $MgO.8NiO.2Fe_2O_4$, $MgO.35NiO.65Fe_2O_4$ and $MgO.5NiO.5Fe_2O_4$ are 25.6nm, 23.6nm, 23.4nm and 48.5nm. The SEM micro-graphs show well-packed and continuous grain structure. Uniformity can be observed along with aggregation of particles to some extent. At the crystallite boundaries, small pores are also observed.
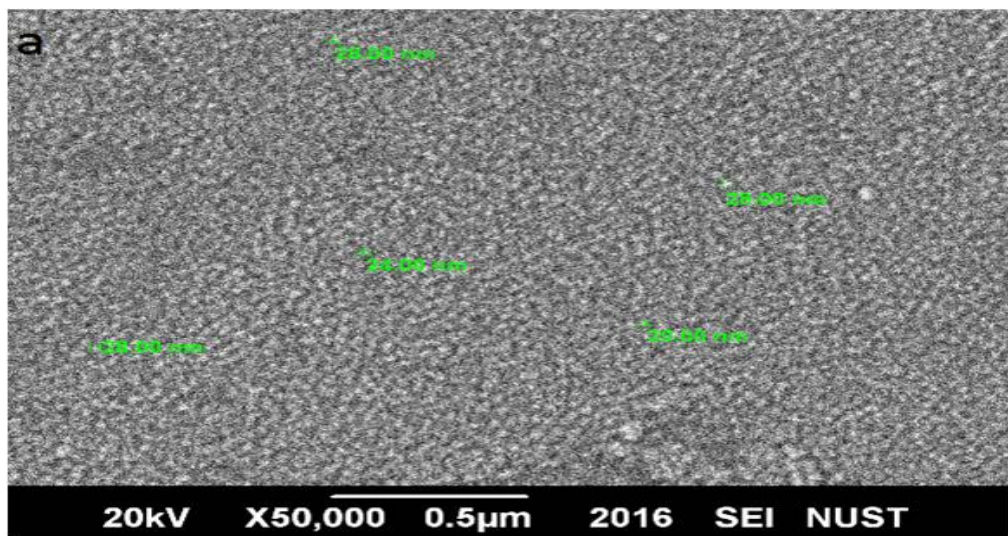
Figure 4.6: SEM images of $Mg_{1-x}Ni_xFe_2O_4$ x = 0.0
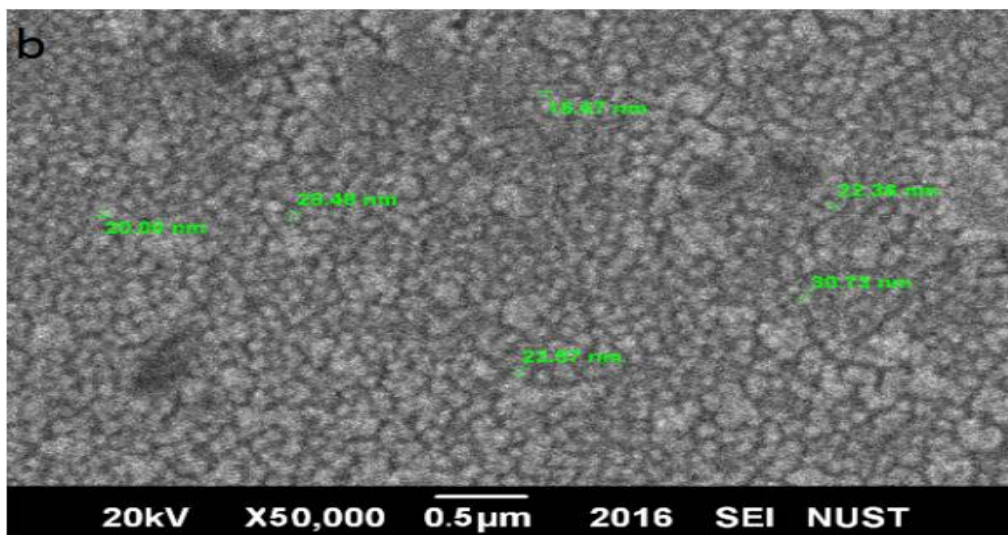
Figure 4.7: SEM images of $Mg_{1-x}Ni_xFe_2O_4$ x = 0.2
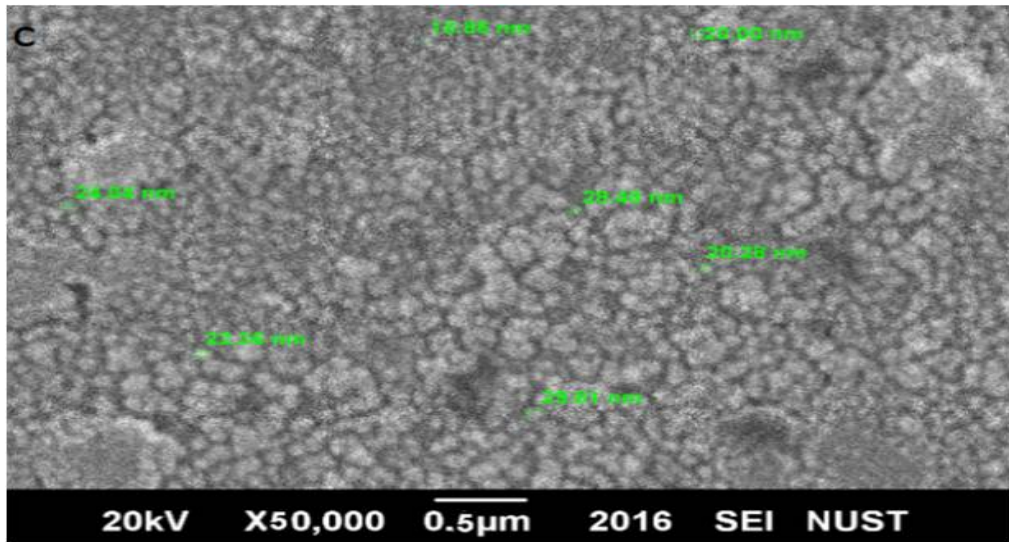
Figure 4.8: SEM images of $Mg_{1-x}Ni_xFe_2O_4$ x = 0.35
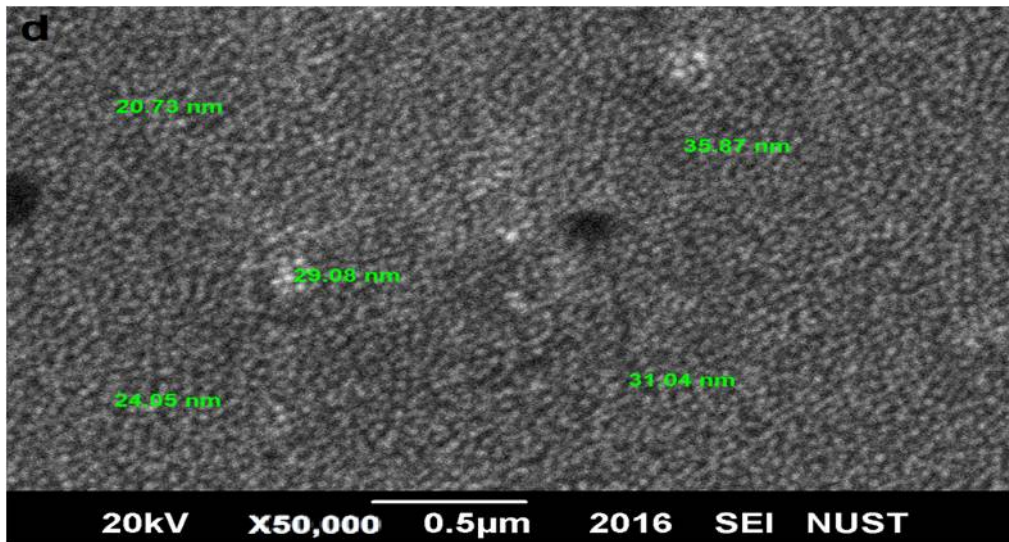
Figure 4.9: SEM images of $Mg_{1-x}Ni_xFe_2O_4$ x = 0.5

4.3 FTIR Analysis

The prepared samples were further investigated through FTIR spectroscopy. The formation of spinel structure is confirmed by FTIR spectral analysis. The FTIR spectra of Mg/Ni ferrites are shown in Figure 4.10.

It can be seen that transmittance is increased with the increase in Ni^{2+} content in magnesium ferrites. In IR spectra of spinels, two main absorption bands of metal-oxygen ions are observed. The spectra are con-
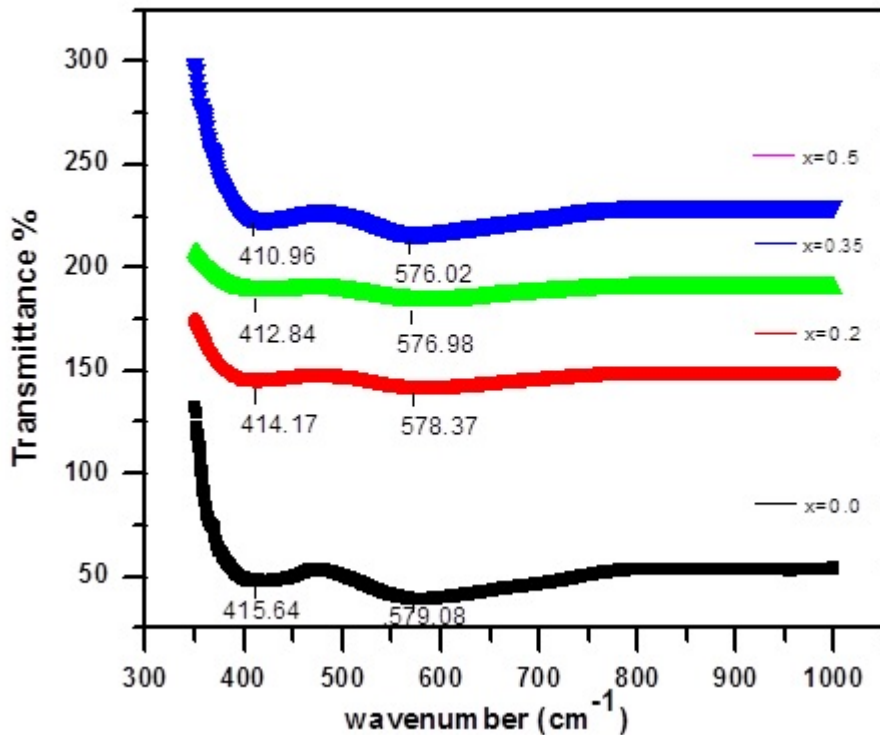
Figure 4.10: FTIR spectra of $Mg_{1-x}Ni_xFe_2O_4$

structed in the wavenumber range of 300-1000 cm^{-1}. In this range bands are consigned to the metal ions vibrations in the crystal lattice [77]. Two bands can be seen in the range of 400-600 cm^{-1}, which are the characteristic feature of spinel structure. The band observed in the high frequency region is referred to the tetrahedral A-site, whereas the one observed in low frequency region is referred to the octahedral B-site as evident from literature [78]. The band at lowest frequency corresponding to ν_1, observed in the range of 410-416 cm-1 for the four samples, is assigned to intrinsic metal-oxygen stretching mode at the octahedral site. The other absorption band ν_2, at highest frequency, corresponds to the metal-oxygen vibrations at the tetrahedral site in the range of 570-580 cm^{-1}. The values observed for these bands are commonly dependent on synthesis conditions and the dopant. Difference of bond length between metal and oxygen atoms is responsible for difference in position of these bands at tetrahedral and octahedral sites. Shift in bands towards lower wave number with increase in Ni^{2+} content in magnesium ferrites is no-

ticed, this can be assosiciated to the increasing distance among cations and anions $Fe^{3+} - O^{2-}$. Values of ν_1 and ν_2 are enlisted in Table 4.2.

$Mg_{1-x}Ni_xFe_2O_4$	x = 0	x = 0.2	x = 0.35	x = 0.5
ν_1 (cm^{-1})	415.64	414.17	412.84	410.96
ν_2 (cm^{-1})	579.08	578.37	576.98	576.03

Table 4.2: Bands observed at tetrahedral and octahedral sites ν_1 & ν_2 for prepared samples

4.4 Dielectric Behavior

4.4.1 Dielectric Constant and Dielectric Loss

The dielectric properties of the pellets made by compressing the synthesized nanoferrites powder were studied. Firstly, the dielectric constant and the dielectric loss were calculated using the values obtained from the LCR meter and were plotted against the logarithm of frequency. The trends are shown in Figures 4.11 and 4.12.

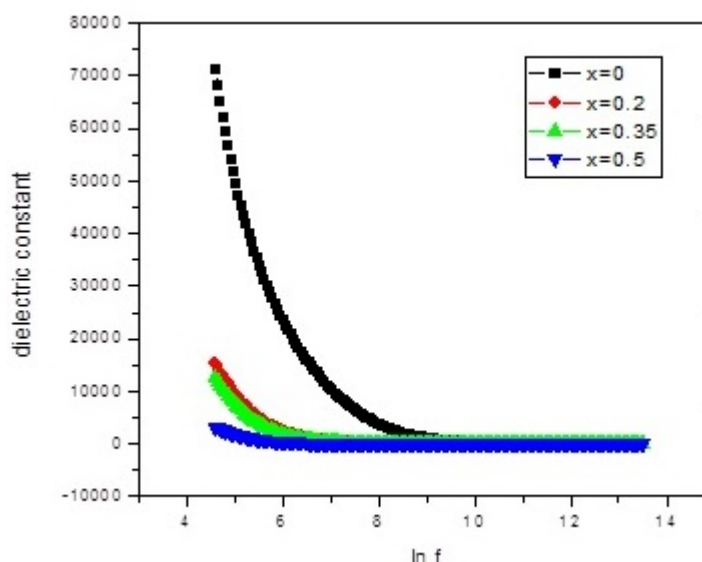**Figure 4.11:** Dielectric constant $Mg_{1-x}Ni_xFe_2O_4$

It can be seen that both dielectric constant and dielectric loss tend to decrease with increasing frequency and almost become constant at a certain value of frequency. This can be explained by the hopping mechanism between the pairs of ions. Electrons arrive at the grain boundaries
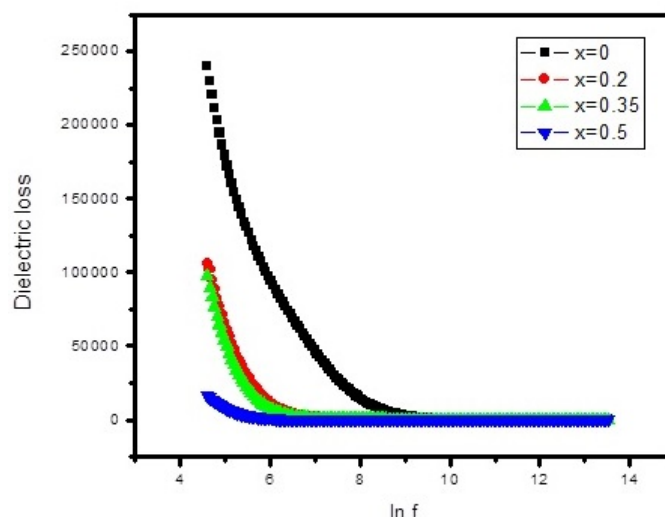
Figure 4.12: Dielectric loss of $Mg_{1-x}Ni_xFe_2O_4$

through hopping and if the resistance is high at grain boundaries, electrons accumulate and polarization occurs. Polarization in spinel ferrites could be understood as the general conduction mechanism. Conversion of ferrous to ferric ions Fe^{2+}/ Fe^{3+} results in movement of electrons in the applied field direction, these electrons are responsible for polarization. By increase in the frequency of the field being applied, electrons tend to reverse their direction. Beyond some specific value of frequency, the electron exchange does not follow the alternating field. As a result, possibility of electrons to reach at the grain boundaries decreases and polarization gets reduced too. Hence, the dielectric constant gets decreased by the increase in frequency of the field [79]. The detailed explanation of inverse relationship between dielectric constant and frequency is provided in Koops phenomenological theory [80], which regards the dielectric material as an inhomogeneous medium in the two layers of the Maxwell-Wagner type model [81]. The decrease in dielectric loss with frequency is normal behavior in ferrites as the ions participating in polarization are lagging behind the applied field at higher frequencies [82]. The dielectric constant and dielectric loss are observed to decrease with increase in the doping concentration.

4.4.2 Tangent Loss

Figure 4.13 shows the tangent loss curve for the prepared samples. It can be observed that tangent loss is also decreasing with frequency. It can be observed that for each sample, tangent loss decreases significantly with the increase in frequency. At increased frequencies of applied field, the frequency of hopping electrons cannot follow the alternating field beyond a certain value, so the loss gets decreased [83]. It can be observed that tangent loss values are also reduced with the increase in dopant.
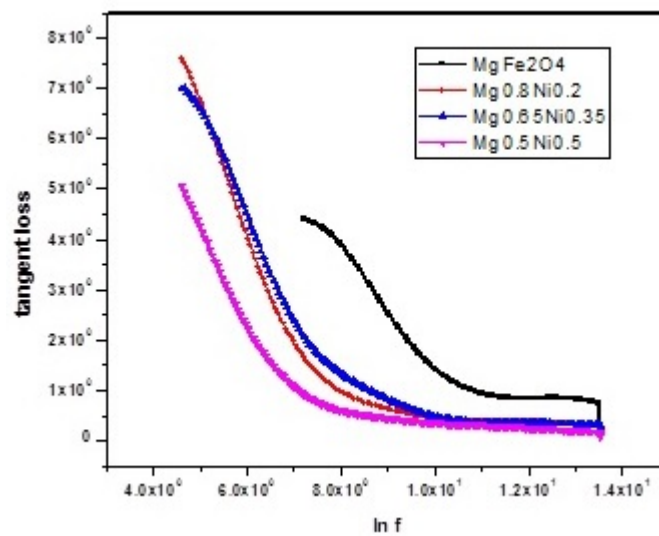
Figure 4.13: Tangent loss of $Mg_{1-x}Ni_xFe_2O_4$

Actually, tangent loss corresponds to the amount of energy being dissipated in the samples in presence of applied field. When loss of energy takes place, there is a shift in phase at certain frequency. Energy losses normally occur when polarization lags behind the field. Therefore, tangent loss decreases at higher frequency.

4.4.3 AC Conductivity

AC conductivity of the samples is shown in the Figure 4.14. An increasing trend of ac conductivity is depicted in the graph. The frequency dependent ac conductivity can also be explained on the basis of Maxwell-Wagner double layer model for dielectrics. At lower frequencies, resistive grain boundaries are more active, whereas, at higher

frequencies, conductive grains become more active and as a result hopping of electrons is enhanced [84, 85]. AC conductivity value is higher for magnesium ferrite and decreases with increase in substituted Ni^{2+} ions.
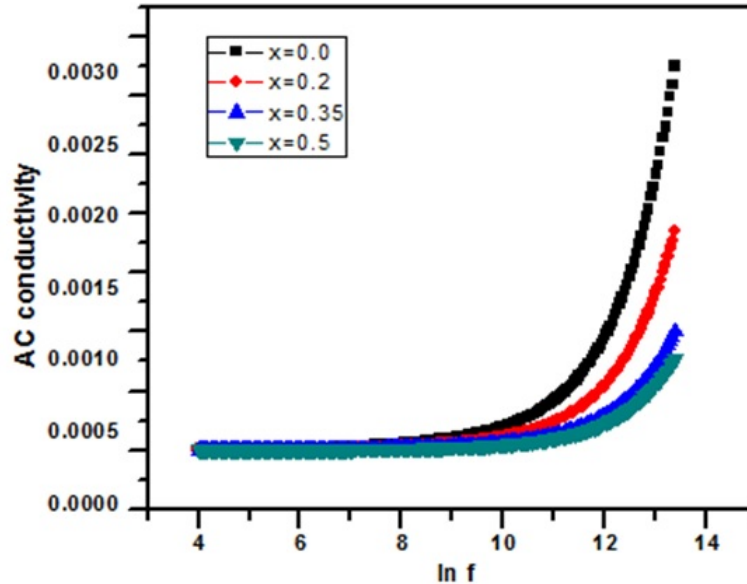
Figure 4.14: AC conductivity of $Mg_{1-x}Ni_xFe_2O_4$

4.4.4   Impedance

Impedance measurements provide useful information about resistive and reactive impedance parts. Figure 4.15 is the representatio of change in real part of impedance against logarithmic frequency at room temerature. It can be observed that impedance (Z) gradually decreases as frequency increases.

With highest doping content of Nickel (x = 0.5), maximum value of (real) impedance is observed. Higher value of resistance corresponds to lower AC conductivity. This is in agreement with AC conductivity behaviour illustrated in Figure 4.15. In other words, AC conductivity and impedance are inversely related.

Cole-cole plot of $Mg_{1-x}Ni_xFe_2O_4$ is shown in Figure 4.16. The imaginary impedance part is plotted against real impedance part. Ideally,

Figure 4.15: Impedance of $Mg_{1-x}Ni_xFe_2O_4$

two semicircles are observed in cole-cole plots. The first semi circle at lower frequencies represents resistance of grain boundaries, whereas resistance of grains is derived from the second semi circle. Incomplete semi circles are evident from cole-cole plot $Mg_{1-x}Ni_xFe_2O_4$
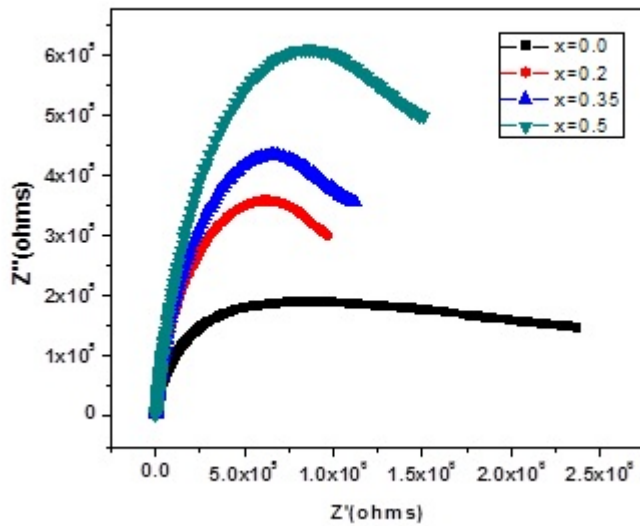
Figure 4.16: Cole-cole plot of $Mg_{1-x}Ni_xFe_2O_4$

4.5   Response Towards Gases
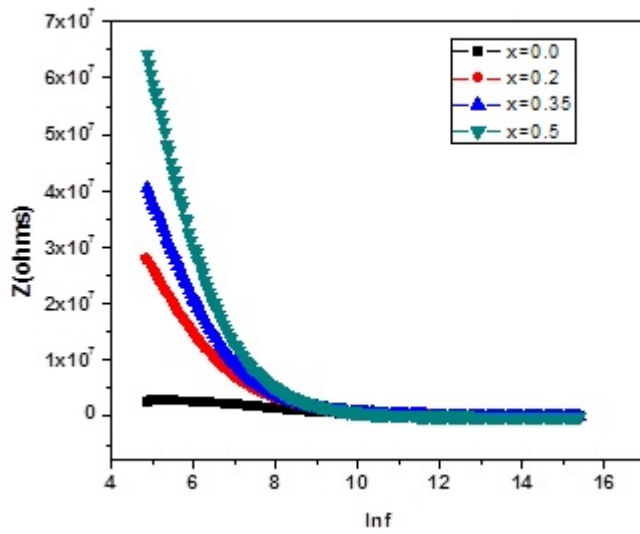
The gas sensing properties of $Mg_{1-x}Ni_xFe_2O_4$ were studied. Sensing of gases is based on the conduction mechanism in ferrites. The adsorption of oxygen at the surface effects the conductance of ferrites. The contact between the sensor element and the gas to be identified determines the gas sensitivity. This contact takes account of the physical and chemical adsorption. The nanoferrites react with oxygen, by shifting electrons from conduction band to the adsorbed oxygen atoms. This results in the formation of ions like O^{2-} or O^-. The oxygen adsorbed on the surface of the sensor converts it into ionic form through some chemical reactions mentioned below [88–90].

$$O_2(gas) \rightarrow O_2(ads)$$
$$O_2(ads) + e^- \rightarrow O^{2-}(ads)$$
$$O_2(ads) + e^- \rightarrow 2O^-(ads)$$
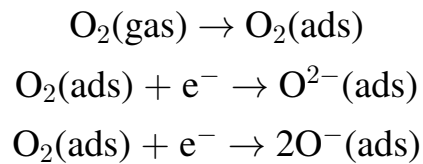
The electrons move from the conduction band to the chemically adsorbed oxygen. This results in reduction of electronic concentration and an increase in resistance is hence noticed.

$$R \rightarrow R(ads)$$
$$R(ads) + O^-(ads) \rightarrow RO(ads) + e^-$$
$$R(ads) + O^{2-}(ads) \rightarrow RO(ads) + 2e^-$$
$$O_2(ads) + e^- \Leftrightarrow 2O^-(ads)$$
$$RO(ads) \rightarrow R(ads)$$
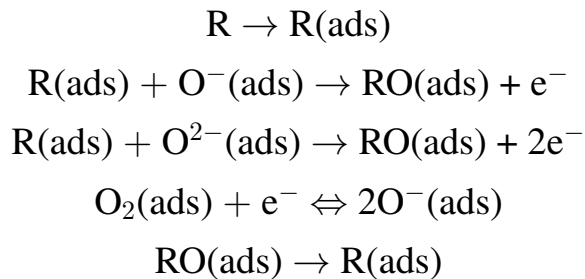
The resistance variation towards N_2, O_2 and CH_4 gases with time is shown in Figures 4.17 - 4.19.
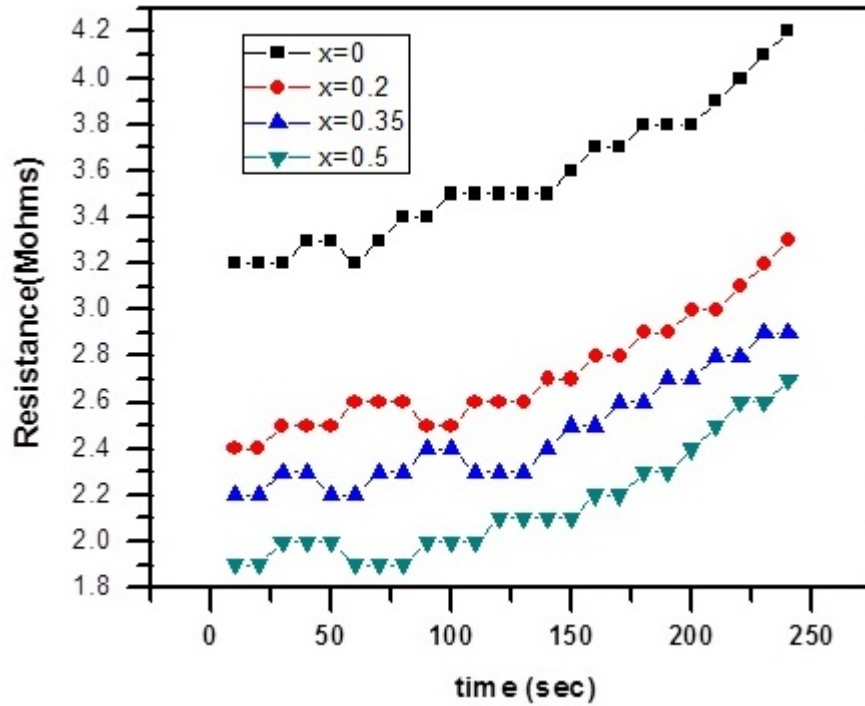
Figure 4.17: Resistance of $Mg_{1-x}Ni_xFe_2O_4$ as a function of time for N_2 gas
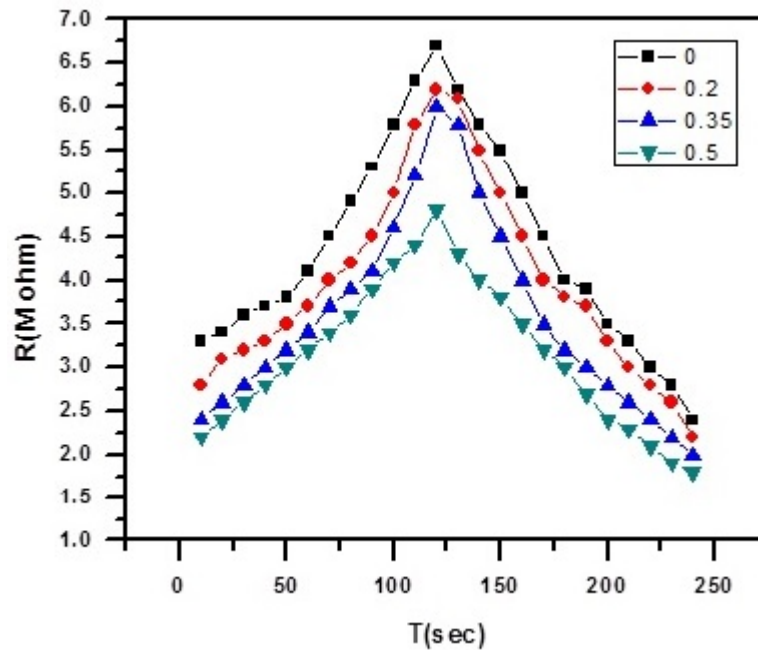
Figure 4.18: Resistance of $Mg_{1-x}Ni_xFe_2O_4$ for O_2 gas

N_2 gas was used as a reference to test the sensing mechanism. It can be observed that resistance is slightly increased upon exposure to N_2 gas. In the case of O_2 and CH_4 gases, firstly, an increase in resistance is observed, then it gets decreased.
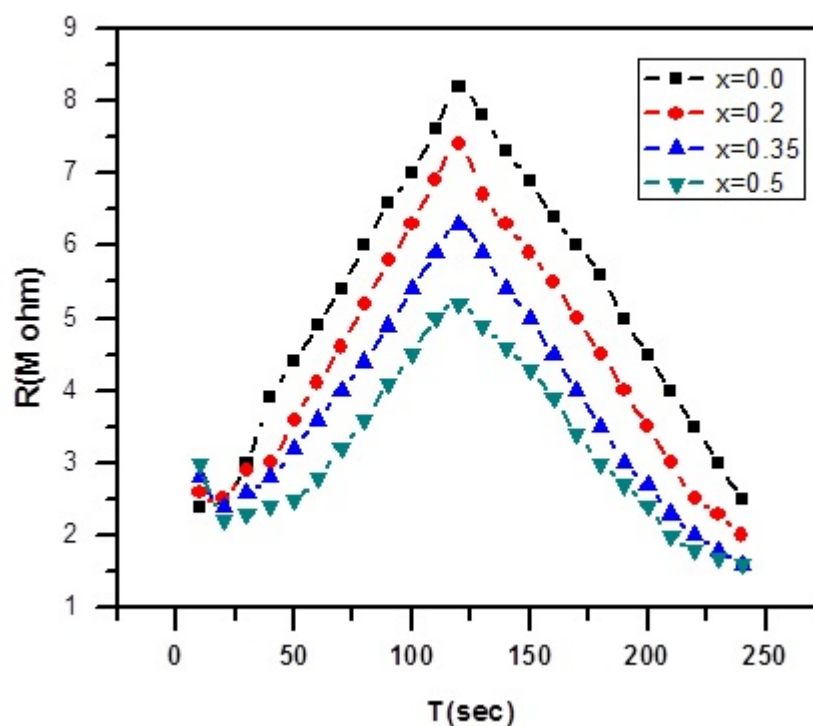
Figure 4.19: Resistance of $Mg_{1-x}Ni_xFe_2O_4$ for CH_4 gas

A comparison in the sensitivities as a function of composition is shown in Figure 4.20 and Table 4.3. Sensitivity towards gases is observed to decrease with increase in doping concentration.

Dopant content (x)	Sensitivity towards CH_4	Sensitivity towards O_2	Sensitivity towards N_2
0.0	1.76	1	0.12
0.2	1.6	0.96	0.1
0.35	1.45	0.84	0.08
0.5	1.39	0.79	0.06

Table 4.3: Sensitivity of $Mg_{1-x}Ni_xFe_2O_4$ towards N_2, O_2 and CH_4 gas
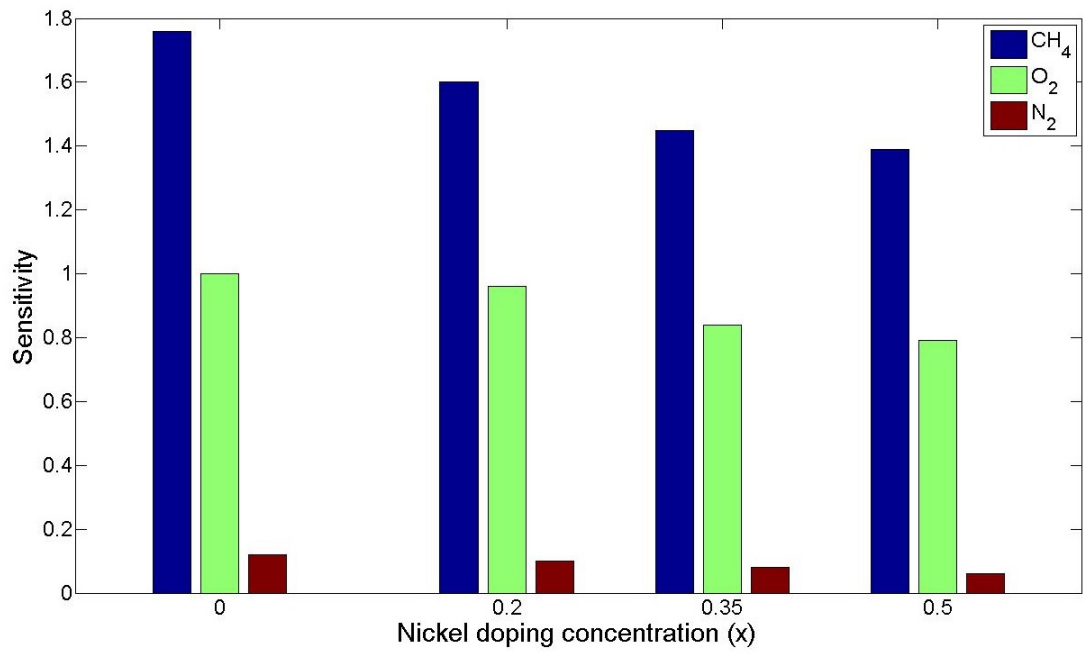
Figure 4.20: Sensitivity of $Mg_{1-x}Ni_xFe_2O_4$ towards N_2, O_2 and CH_4 gas (x=0, 0.2, 0.35 ,x=0.5)

Chapter 5

Conclusions

Nickel doped Magnesium ferrite nanoparticles were prepared in four different compositions. Synthesis approach of co-precipitation was adopted for fabrication of

$Mg_{1-x}Ni_xFe_2O_4$ (x = 0.0, 0.2, 0.35, 0.5) XRD of prepared samples was done to identify the crystal structure. Face centered cubic structure was confirmed by XRD analysis. Considering the most intense peak, crystallite sizes were calculated using the Scherer formula. The lattice constant (a) of the synthesized material was estimated. It is observed that lattice constant decreases with increase in Ni content. The decrease in lattice constant can be attributed to the smaller ionic radius of Ni^{2+} as compared to Mg^{2+}. The mass densities and X-ray densities were calculated using the obtained data. An increase in mass density was observed with increase in the doping content. This increase may be due to greater atomic weight of Ni^{2+} as compared to Mg^{2+}. X-ray density also showed an increasing trend with increase of the dopant. Values of X-ray densities are found to be higher than the mass densities. This is due to presence of the pores which further depends on the sintering environments. The increase in X-ray density may be attributed to the fact that nickel has greater density and atomic concentration as compared to magnesium.

Structure of spinel ferrites was also confirmed through FTIR spectroscopy. Formation of bands is observed in the range of 410-416 cm^{-1} and 570-

580 cm^{-1} at the octahedral and tetrahedral sites respectively. Morphology of the prepared samples was studied by the SEM images. Dielectric properties were also analyzed. Dielectric constant and dielectric loss depicted a decreasing trend with increase in frequency. Tangent loss also tends to decrease with the increasing frequency. AC conductivity of the samples showed an increasing trend with the increase in frequency. Gas sensing properties of the samples with different compositions were also studied. It was observed that sensitivity of a gas was increased with increase in the doping content. N$_2$, O$_2$ and CH$_4$ gases were used. Mg$_{1-x}$Ni$_x$Fe$_2$O$_4$ showed greater sensitivity towards methane gas. The synthesized material can be potential candidates to be used as gas sensors in future.

References

[1] N. Kumar, S. Kumbhat, Essentials in Nanoscience and Nanotechnology, Wiley 2016

[2] A. Dowling, Nanoscience and Nanotechnologies: opportunities and uncertainties, Latimer Trend Ltd., 2004

[3] M.H. Fulekar, Nanotechnology: Importance and Applications, I K International Publishing House, New Delhi, 2010

[4] K.K. Chattopadhyay, A.N. Banerjee, Introduction to Nanoscience and Nenotechnology, PHI Learning, New Delhi, 2009

[5] P. Dutta, S. Gupta, Understanding of Nano Science and Technology, Global Vision Publishing House, New Delhi, 2006

[6] M.F. Ashby, P.J. Ferreira, D.L. Schodek, Nanomaterials, Nanotechnologies and Design: An Introduction for Engineers and Architects, Elsevier, Paris 2009

[7] M. Niederberger, N. Pinna, Metal Oxide Nanoparticles in Organic Solvents: Synthesis, Formation, Assembly and Application, Springer 2009

[8] S.C. Tjong, Nanocrystalline Materials: Their Synthesis-Structure-Property Relationships and Applications, Elsevier 2013

[9] A. Alagarasi, Introduction to nanomaterials, National center for catalysis research, Madras, 2011

[10] G.L. Hornyak, H.F. Tibbals, J. Dutta, J.J. Moore, Introduction to Nanoscience and Nanotechnology, CRC Press 2008

[11] A. Surendiran, S. Sandhiya, S.C. Pradhan, C. Adithan, Novel applications of nanotechnology in medicine, International Journal of Medical Research, 2009

[12] M.C. Santos, O. Kesler, A.L.M. Reddy, Nanomaterials for Energy Conversion and Storage, Journal of Nanomaterials, 2012

[13] G. David, Nanotechnology for clean water: Facts and figures, SciDev.Net, 2009

[14] S.R. Mousavi, M. Rezaei, Nanotechnology in Agriculture and Food Production, Journal of Applied Environmental and Biological Sciences, 2011

[15] S. Raj, S. Jose, U.S. Sumod, M. Sabitha, Nanotechnology in cosmetics: Opportunities and challenges, Journal of Pharmacy and Bio allied Sciences, 2012

[16] http://www.nanoandme.org/nano-products/paints-and-coatings

[17] V. Mlinar, Nanotechnology 24, 042001, 2013

[18] J. Shi, Y. Zhu, X. Zhang, W.R.G. Baeyens, A.M. Garca-Campana, TrAC Trends in Analytical Chemistry, 2004

[19] S. Besner, M. Meunier, Laser Precision Microfabrication, Springer, 2010

[20] J.C. Colmenares, R. Luque, J.M. Campelo, F. Colmenares, Z. Karpioski, A.A. Romero, Materials, 2 (2009) 2228

[21] L. Feng, Z. Liu, Nanomedicine 6 (2011) 317

[22] T.J. Simmons, Nanomaterials for BiomedicineAmerican Chemical Society, 2012

[23] K. Habiba, V.I. Makarov, B.R. Weiner, G. Morell, Fabrication of Nanomaterials by Pulsed Laser Synthesis: Manufacturing Nanostructures, OCN, 2014

[24] Z. Yao, C. Dekker, P. Avouris, Carbon Nanotubes, Springer, 2001

[25] M. Suzuki, N. Kawamura, H. Miyagawa, J.S. Garitaonandia, Y. Yamamoto, H. Hori, Physical Review Letters, 108 (2012) 047201

[26] R. Valenzuela , Novel applications of ferrites, Physics Research International, 2012

[27] R. Valenzuela, Magnetic ceramics, Cambridge University Press, 2005

[28] J.F. Hochepied, M.P. Pileni, Magnetic properties of mixed cobaltzinc ferrite nanoparticles, Journal of Applied Physics, 2000

[29] S. Shakoor , M.N. Ashiq, M.A. Malana, A. Mahmood, M.F. Warsi, M. Najam-ul-Haq, N. Karamat, Electrical, dielectric and magnetic characterization of BiCr substituted M-type strontium hexaferrite nanomaterials. Journal of Magnetism and Magnetic Materials. 2014

[30] A.J. Moulson, J.M. Herbert, Electroceramics: materials, properties, applications, John Wiley & Sons, 2003

[31] K.C. Patil, Chemistry of nanocrystalline oxide materials: combustion synthesis, properties and applications, World Scientific, 2008

[32] D.S. Mathew, R.S. Juang, An overview of the structure and magnetism of spinel ferrite nanoparticles and their synthesis in microemulsions, Chemical Engineering Journal, 2007

[33] D.C. Jiles, Introduction to magnetism and magnetic materials, Chapman and Hall, 1991

[34] R.C. Pullar, Hexagonal ferrites: a review of the synthesis, properties and applications of hexaferrite ceramics, Progress in Materials Science, 2012

[35] A. Goldman, Recent advances in ferrite materials technology, Modern Ferrite Technology, 1990

[36] R.J. Tilley, Understanding solids: the science of materials. John Wiley & Sons, 2004

[37] M.G. Naseri, E.B. Saion, Crystallization in spinel ferrite nanoparticles, Advances in Crystallization Processes, 2012

[38] M. Pardavi-Horvath, Microwave applications of soft ferrites, Journal of Magnetism and Magnetic Materials, 2000

[39] G. Winkler, Crystallography, chemistry and technology of ferrites, Magnetic properties of Materials, McGraw-Hill, 1971

[40] N.A. Spaldin Magnetic materials: fundamentals and device applications, 2003

[41] P. Tenaud, A. Morel, F. Kools, J.M. Le-Breton, L. Lechevallier, Recent improvement of hard ferrite permanent magnets based on La-Co substitution, Journal of alloys and compounds, 2004

[42] S.H. Yu , T. Fujino, M. Yoshimura, Hydrothermal synthesis of $ZnFe_2O_4$ ultrafine particles with high magnetization, Journal of Magnetism and Magnetic Materials, 2003

[43] H. Deng, X. Li, Q. Peng, X. Wang, J. Chen, Y. Li, Monodisperse magnetic single crystal ferrite microspheres, Angewandte Chemie, 2005

[44] J.A.L. Perez, M.A.L. Quintela, J. Mira, J. Rivas, S.W. Charles, Advances in the preparation of magnetic nanoparticles by the microemulsion method, The Journal of Physical Chemistry B, 1997

[45] Q. Chen, Z.J. Zhang, Size-dependent superparamagnetic properties of $MgFe_2O_4$ spinel ferrite nanocrystallites, Applied physics letters, 1998

[46] Z.X. Tang, C.M. Sorensen, K.J. Klabunde, G.C. Hadjipanayis, Preparation of manganese ferrite fine particles from aqueous solution, Journal of colloid and interface science, 1991

[47] C.T. Seip, E.E. Carpenter, C.J. O'Connor, V.T. John, S. Li, Magnetic properties of a series of ferrite nanoparticles synthesized in reverse micelles, IEEE Transactions on Magnetics, 1998

[48] J.F. Hochepied, P. Bonville, M.P. Pileni, Nonstoichiometric zinc ferrite nanocrystals: syntheses and unusual magnetic properties, The Journal of Physical Chemistry B, 2000

[49] C. Liu, B. Zou, A.J. Rondinone, Z.J. Zhang, Reverse micelle synthesis and characterization of superparamagnetic $MnFe_2O_4$ spinel ferrite nanocrystallites, The Journal of Physical Chemistry B, 2000

[50] M.P. Gonzalez-Sandoval, A M. Beesley, M. Miki-Yoshida, L. Fuentes-Cobas, J.A. Matutes-Aquino, Comparative study of the microstructural and magnetic properties of spinel ferrites obtained by co-precipitation, Journal of Alloys and Compounds, 2004

[51] A. Sutka, G. Mezinskis, Sol-gel auto-combustion synthesis of spinel-type ferrite nanomaterials, Frontiers of Materials Science, 2012

[52] V. Pillai, D.O. Shah, Synthesis of high-coercivity cobalt ferrite particles using water-in-oil microemulsions, Journal of Magnetism and Magnetic Materials, 1996

[53] T.P. Almeida, M.W. Fay, Y. Zhu, P.D. Brown, Hydrothermal synthesis of mixed cobalt-nickel ferrite nanoparticles, Journal of Physics: Conference Series, 2012

[54] P. Ravindranathan, K.C. Patil, Novel solid solution precursor method for the preparation of ultrafine Ni-Zn ferrites, Journal of Materials Science, 1987

[55] H. Igarash, K. Okazaki, Effects of Porosity and Grain Size on the Magnetic Properties of NiZn Ferrite, J. Am. Ceram. Soc, 1977

[56] A. Goldman. Understanding ferrites. American Ceramic Society Bulletin, 1984

[57] D. Stoppels, Developments in soft magnetic power ferrites, Journal of Magnetism and Magnetic Materials, 1996

[58] K.H. Lee, D.H. Cho, S.S. Jeung, Ni-Zn ferrite spinel: characterization and evaluation of its suitability for ion selective electrodes, Journal of materials science letters, 1997

[59] C.S. Kim, Y.S. Yi, K.T. Park, H. Namgung, J.G. Lee, Growth of ultrafine CoMn ferrite and magnetic properties by a solgel method, Journal of applied physics, 1999

[60] R. Peelamedu, C. Grimes, D. Agrawal, R. Roy, P. Yadoji, Ultralow dielectric constant nickelzinc ferrites using microwave sintering, Journal of materials research, 2003

[61] A.K.H. Hossain, M. Seki, T. Kawai, H. Tabata, Colossal magnetoresistance in spinel type $Zn_{1-x}Ni_xFe_2O_4$, Journal of applied physics, 2004

[62] A. Goldman, Handbook of Modern Ferromagnetic Materials, Kulwer Acad. Pub, 1999

[63] L. Neel, Magnetic properties of ferrites; Ferrimagnetism and anti ferromagnetism, Ann. Phys. 1948

[64] J. Govha, T.B. Narsaiah, P. Kumar, C.S. Chakra, Synthesis of Nano-Magnesium Ferrite Spinel and its Characterization, International Journal of Engineering Research & Technology, 2014

[65] Sugimoto M., The past, present, and future of ferrites, Journal of the American Ceramic Society, 1999

[66] M. Karmakar, P. Das, M. Pal, B. Mondal, Acetone and ethanol sensing characteristics of magnesium zinc ferrite nano-particulate chemi-resistive sensor, Journal of Materials Science, 2014

[67] N. Rezlescu, N. Liftimie, E. Rezlescu, C. Doroftie, Semiconducting gas sensor for acetone based on the fine grained nickel ferrite, Sensors and Actuators B: Chemical, 2006

[68] C. Suryanarayana, M.G. Norton, X-ray diffraction: a practical approach, Springer Science & Business Media, 2013

[69] Klug, H. Philip, L.E. Alexander, X-ray diffraction procedures, 1954

[70] Moore, D. Milton, R.C. Reynolds, X-ray Diffraction and the Identification and Analysis of Clay Minerals, Oxford university press, 1989

[71] L. Lou, Introduction to Phonons and Electrons, World Scientific 2013

[72] M. Aliuzzaman, M.M Haque, M.J. Ferdous, Effect of Sintering Time on the Structural, Magnetic and Electrical Transport Properties of $Mg_{0.35}Cu_{0.20}Zn_{0.45}Fe_{1.94}O_4$ Ferrites, World Journal of Condensed Matter Physics, 2014

[73] A. Khursheed, Scanning Electron Microscope Optics and Spectrometer, 2010

[74] J.L. Koenig, Spectroscopy of Polymers, Elsevier Science & Technology, 1999

[75] http://www.buzzle.com/articles/lcr-meter-working-principle-and-uses.html

[76] http://www.radio-electronics.com/info/t-and-m/lcr-meter/basics-tutorial.php

[77] A. Baykal, N. Kasapoglu, Y. Koseoglu, M.S. Toprak, CTAB-assisted hydrothermal synthesis of $NiFe_2O_4$ and its magnetic characterization, Journal of Alloys and Compounds, 2008

[78] M. Salavati-Niasari, F. Davar, T. Mahmoudi, A simple route to synthesize nanocrystalline nickel ferrite ($NiFe_2O_4$) in the presence of octanoic acid as a surfactant, Polyhedron, 2009

[79] S. Assar, H. Abosheiasha, M. El-Nimr, Study of the dielectric behavior of CoNiLi nanoferrites, Journal of Magnetism and Magnetic Materials, 2014

[80] C. Koops, On the dispersion of resistivity and dielectric constant of some semiconductors at audiofrequencies, Physical Review, 1951

[81] R. Kambale, P.A. Shaikh, C.H. Bhosale, Dielectric properties and complex impedance spectroscopy studies of mixed NiCo ferrites, Smart Materials and Structures, 2009

[82] Y. Kseolu, M. Bay, M. Tan, A. Baykal, H. Sozeri, Magnetic and dielectric properties of $MnO.2NiO.8Fe_2O_4$ nanoparticles synthesized by PEG-assisted hydrothermal method, Journal of Nanoparticle Research, 2011

[83] E. Melagiriyappa, H. Jayanna, B. Chougule, Dielectric behavior and AC electrical conductivity study of Sm^{3+} substituted MgZn ferrites, Materials chemistry and physics, 2008

[84] C. Murugesan, M. Perumal, G. Chandrasekaran, Structural, dielectric and magnetic properties of cobalt ferrite prepared using auto combustion and ceramic route, Physica B: Condensed Matter, 2014

[85] K. Verma, A. Kumar, D. Varshney, Dielectric relaxation behavior of $A_xCo_{1-x}Fe_2O_4$ (A= Zn, Mg) mixed ferrites, Journal of Alloys and Compounds, 2012

[86] S.K. Durrani, S. Naz, M. Mehmood, M. Nadeem, Structural, impedance and Mssbauer studies of magnesium ferrite synthesized via solgel auto-combustion process, Journal of Saudi Chemical Society, 2016

[87] M. Mosleh, Synthesis, characterization and optical properties of neodymium doped nickel ferrite nanoparticles prepared by novel solgel method, Journal of Materials Science: Materials in Electronics, 2016

[88] P. Hankare, S.D. Jadhav, U.B. Sankpal, R.P. Patil, Gas sensing properties of magnesium ferrite prepared by co-precipitation method, Journal of Alloys and Compounds, 2009

[89] G. Zhang, M. Liu, Effect of particle size and dopant on properties of SnO_2-based gas sensors. Sensors and Actuators B: Chemical, 2000

[90] R. Waghulade, P. Patil, R. Pasricha, Synthesis and LPG sensing properties of nano-sized cadmium oxide. Talanta, 2007